THE UNIVERSITY OF MICHIGAN

College of Engineering
Department of Aeronautical and Astronautical Engineering

Technical Report

EXPERIMENTAL INTERACTION EFFECTS OF FORWARD-LOCATED SIDE JETS ON A BODY OF REVOLUTION

James L. Amick

Warren Stubblebine

Paul C. Y. Chen

WTM - 276

ORA Project 05194

under contract with:

HERCULES POWDER COMPANY
ALLEGANY BALLISTICS LABORATORY
RESEARCH AND DEVELOPMENT SUBCONTRACT NO. 205

administered by:

THE UNIVERSITY OF MICHIGAN OFFICE OF RESEARCH ADMINISTRATION
ANN ARBOR

March 15, 1963

ABSTRACT

Experimental results are presented for a supersonic jet issuing perpendicularly from a sphere-cone-cylinder body into main streams having Mach numbers of 0, 0.6, 1.9, and 4.0. Moment and force increments due to the jet, non-dimensionalized by means of corresponding quantities in a vacuum, are shown as functions of the jet stagnation pressure ratio. Effects of angle of attack, jet location, and body length are also displayed. The adverse interaction effect is found to reduce the jet effectiveness to one-sixth of its value in a vacuum, for an extreme case at Mach number 1.9. A few pressure measurements are presented, which show that a low pressure region behind the jet is the apparent cause of the adverse interaction.

TABLE OF CONTENTS

LIST OF FIGURES

LIST OF FIGURES (CON'D)

LIST OF SYMBOLS

a	speed of sound
a_{o_j}	jet stagnation speed of sound
A	nozzle cross-section area in plane of base of plug
A_b	area of base of plug ($= \pi r_1^2$)
I_s	specific impulse of normal force due to jet ($= N_\Delta / \dot{m}$)
$I_{s_{vac}}$	specific impulse of jet in vacuum ($= N_{vac} / \dot{m}$)
$\dot{m}$	mass flow rate
M	free stream Mach number
M'	Mach number on toroidal control surface ($\overset{\frown}{ad}$ in Fig. 3)
M_s	specific moment due to jet ($= M_\Delta / \dot{m}$)
$M_{s_{vac}}$	specific moment due to jet issuing into vacuum from nozzle located 0.4 diameters aft of nose
M_Δ	increment in moment due to jet, including interaction effects. (Moment in flow with jet on, minus moment with jet off. Moment center is 5.31 body diameters from nose.)
N_{vac}	normal force of jet issuing into vacuum
N_Δ	increment in normal force due to jet, including interaction effects. (Normal force on body in flow with jet on, minus normal force in flow with jet off.)
p	pressure
p'	pressure on toroidal control surface ($\overset{\frown}{ad}$ in Fig. 3)
p_1	free stream static pressure
p_a	ambient pressure (pressure at nozzle exit with jet off.)
p_b	pressure on base of plug
p_{o_j}	jet stagnation pressure
r_1	radius of base of plug (Fig. 3)
r_2	radius of cylindrical surface of nozzle (Fig. 3)
V	velocity
α	angle of attack
γ	ratio of specific heats of jet gas
ρ	mass density

INTRODUCTION

Attitude control jets located near the nose of a body of revolution can have several advantages over rearward-located jets. For example, the moment arm between a forward-located jet and the center of gravity is sometimes much greater than that of a rear jet. Also, with a jet located near the nose, wind forces can be counteracted without developing large bending moments in the structure of a missile, since the center of pressure for a finless body is near the nose.

A disadvantage of nose jets is the adverse interaction effect (Reference 1). When a nose jet issues into a moving airstream its effective thrust is reduced by the pressure field developed on the body. For an aft jet this reduction in thrust does not occur at supersonic speeds.

The present investigation was conducted for the purpose of evaluating the adverse interaction effect for nose jets located at different axial distances from the nose, and at various free stream Mach numbers. The investigation consisted primarily of force and moment measurements at Mach numbers 0, 0.6, 1.9, and 4.0. A limited number of pressure measurements were made on the body in the vicinity of the jet.

APPARATUS AND TESTS

The University of Michigan 8- by 13-inch supersonic wind tunnel was employed to obtain the experimental results of this report. This tunnel is vacuum driven with either atmospheric or subatmospheric stagnation pressure. The tests were conducted at Mach numbers of 0, 0.6, 1.9, and 4.0 and at Reynolds numbers varying from 42,200 to 343,000 per inch.

The model consisted of a sphere-cone-cylinder forebody with three removable cylindrical afterbody extensions (See Figure 1). With all the afterbody extensions in place, the model had a length-to-diameter ratio of $\frac{L}{D} = 7.0$. Removing successive extensions reduced this ratio to 5.04, 3.52, and 2.52.

The jet issued from the body in a direction perpendicular to the axis, at any of the four locations indicated in Figure 1. At each of these locations a cylindrical hole was drilled thru the wall thickness of the model. A modified plug nozzle was then formed by inserting a plug, as shown in Figure 2, into one of these holes. The throat of this plug nozzle was formed by the annular space between the maximum diameter of the plug and the inside diameter of the hole. The three unused holes were plugged. As a result, the force due to the jet could be measured for the different jet locations.

The jet gas was laboratory air, and the jet stagnation pressure was varied from 112 psia to 12 psia by throttling the air flow to the jet. This produced a maximum force of approximately .3 pound with the plug nozzle, whose throat area was .00166 square inches.

Normal force and moment data were obtained from a hollow sting balance through which the air flowed to the jet. Strain gages, bonded on the sting at three locations, responded to changes in bending moment

caused by the jet forces. The outputs of the strain gages were amplified and recorded by an oscillograph. Frequent calibrations were conducted by hanging weights from a pivot centered in a plug inserted in the jet nozzle.

The increment in normal force or moment produced by the jet was measured by turning off the jet during each run. The difference between the normal force with the jet on and the normal force with the jet off is the increment in normal force due to the jet. In order to shut off quickly the airflow to the jet, a 3/4" solenoid valve was mounted as close to the model as possible. The reference jet reaction was obtained by operating the jet in the evacuated tunnel. The normal force thus measured was taken to be the jet reaction force in a vacuum. The importance of the reference jet reaction will be discussed in the Data Reduction section of this report.

Measurements were also made of the mass flow of air through the jet. These measurements were made by means of a thin plate orifice and manometer tubes which measured the pressure differential across the orifice. It is interesting to note that during the actual testing a comparison of results for different parts of the experiment could indicate partial blockage of the nozzle throat by dirt particles. When blockage occurred the nozzle plug was removed, cleaned, and reinstalled.

Tests were conducted on the model for variations in Mach number, angle of attack, jet stagnation pressure, and number of afterbody extensions in order to determine the effect of each change. The variations of both Mach number and jet stagnation pressure have already been mentioned. Various positive and negative angles of attack were tested up to a maximum of ten degrees. The model was tested primarily with all extensions, but one or more of the three removable sections were removed for several tests.

The tests at Mach number 0.6 were made with the Mach number 1.4 nozzle blocks installed. A gate valve at the downstream end of the tunnel was set in a partially open position, so that it formed a sonic throat and controlled the Mach number in the test section. The measured test section Mach number varied from 0.52 to 0.63, increasing with tunnel stagnation pressure.

Schlieren pictures were taken to observe the effects of the jet upon the boundary layer and to determine certain characteristics of the flow field. China clay was also employed to determine the characteristics of the flow field on the surface of the model.

For pressure tests the nosepiece of the model was replaced by one having the same overall dimensions and containing 11 pressure orifices. Eight of these were located forward of the jet nozzle station. The other three pressure orifices were located behind the jet in a separate section. The two sections could be independently rotated about the body axis to change the orientation of the three rear orifices with respect to the jet.

The pressure tests were made at Mach number 1.9, and at a zero angle of attack. Only one jet location was used for the pressure tests, so that a maximum number of pressure taps could be accomodated. The location chosen was 0.90 diameters from the nose.

The pressures on the model as well as the tunnel stagnation pressure were measured on a mercury manometer board. Mass flow data was obtained in the same manner as in the force tests.

DATA REDUCTION

The normal force and moment increments due to the jet were divided by the measured mass flow to obtain specific impulse and specific moment. These specific values were then nondimensionalized by dividing by the corresponding quantities for a jet discharging into a vacuum. It was therefore necessary to determine the jet specific impulse in a vacuum.

A theoretical value for the vacuum specific impulse, based on the flow model shown in Figure 3, is derived in Appendix A. In order to obtain an experimental value of this quantity the zero Mach number, tunnel-evacuated data were plotted in Figure 4 as values of measured specific impulse plus the ambient pressure effect correction, according to equation (B5) of Appendix B. From this plot a value of 68.5 was chosen for $I_{s_{vac}}$, to be used in all subsequent data reduction. Note that this is about one percent less than the estimated value from Appendix A.

The data were corrected for a pressure sensitivity of the rearmost strain gage bridge. An asymmetry of the hollow sting balance results in an indicated moment at this bridge when the sting is pressurized. The measured increments of moment at this station due to turning the jet off, therefore, contain an error resulting from the sting pressure sensitivity. This error either subtracts from or adds to the true change in moment due to the jet force, depending on whether the sting is in the normal position or inverted 180°, with respect to the jet direction. For the jet nozzle used in this investigation the correction to the indicated moment at the rearmost strain gage station was about 5%.

The center of moments for the data presented in this report is the rearmost strain gage station, 5.31 body diameters aft of the nose. This center was chosen because it is a reasonable center of gravity location,

and required a minimum of data reduction. Values of specific moment ratio were obtained from the measured moment at the rearmost strain gage station by dividing by the vacuum specific impulse and the measured mass flow, and multiplying by the distance from the rearmost strain gage station to the most forward jet location (0.4 body diameters aft of the nose). Thus the specific moment ratio is merely the ratio of the measured moment to the moment produced by a jet discharging into vacuum at the same mass flow rate from a geometrically similar nozzle 0.4 body diameters aft of the nose.

The specific moment ratio data can be easily transferred to any other moment center by means of the following relation:

$$\frac{M_s'}{M_{s_{vac}}'} = \frac{M_s}{(N_{vac}/\dot{m})\,x} - \frac{(N_\Delta/\dot{m})(5.31-x)}{(N_{vac}/\dot{m})\,x} = \frac{M_s}{M_{s_{vac}}}\,\frac{5.31}{x} - \frac{I_s}{I_{s_{vac}}}\,\frac{(5.31-x)}{x} \qquad (1)$$

where M_s is the specific moment (i.e., ratio of moment to mass flow); $M_{s_{vac}}$ is the specific moment of a geometrically similar nozzle located 0.4 body diameters aft of the nose and discharging to a vacuum; x is the distance, in body diameters, from the nose to the new moment center; and the primes denote quantities referred to the new moment center.

RESULTS AND DISCUSSION

Moments and Forces. The main results of the tests are presented in Figure 5 as specific moment ratios. These ratios measure the performance of the control jet in producing a moment about a center 5.31 body diameters aft of the nose, in terms of the moment of a jet issuing into a vacuum at the same mass flow rate from a geometrically similar nozzle located 0.4 body diameters aft of the nose. The data are plotted versus the ratio of jet stagnation pressure to test section static pressure, which, for a given nozzle, is proportional to the ratio of jet force in a vacuum to

a reference aerodynamic force. (Parameters similar to this one gave good correlation of jet interaction data in References 2 and 3.)

Theoretical curves which take account only of the ambient pressure effect (see Appendix B) are also shown in Figure 5. These curves agree very well with the experimental results at Mach number zero, for pressure ratios greater than about 30. At pressure ratios less than 30 it is believed that separation occurs within the nozzle, causing the nozzle thrust to be greater than that given by the theory, which assumes the nozzle to be flowing full.

For the more rearward jet locations, the data at the higher pressure ratios fall below the theoretical curves, probably because of flow induced by the jet. This induced flow tends to reduce pressures on the body in the neighborhood of the jet, and increases pressures on the opposite side of the body. The resulting body pressure distribution decreases the net force of the jet, especially for the more rearward jet locations which are closer to the center of plan form area of the body.

As Mach number increases, the ambient pressure effect becomes less significant, and interaction effects become important. At supersonic speeds the intermediate jet locations give the largest control moments, because the adverse interaction effects are not as serious at these locations as for the most forward jet location.

Specific impulse ratio data are presented in Figure 6. These data enable the specific moment ratio data to be converted to any other moment center, by means of equation (1). The specific impulse ratio can also be thought of as a force effectiveness factor, indicating the ratio of the normal force due to the jet (including interaction effects) to the normal force of a jet issuing into vacuum thru a geometrically similar nozzle at

the same mass flow rate.

Angle of attack effects are shown in Figure 7. At the subsonic speed the moment produced by the jet is reduced as angle of attack increases (jet issuing on leeward side of body). On the other hand, at supersonic speeds the general trend is to increasing effectiveness at higher angles of attack.

Effects of afterbody length are presented in Figure 8, for a jet located 0.9 body diameters from the nose. Again, opposing trends are evident at subsonic and at supersonic speeds, at these particular jet pressure ratios. At the subsonic speed, increasing the body length from 2.5 to 5 diameters increases the specific moment ratio, whereas at supersonic speeds there is a decrease in moment for the same increase in body length.

A turbulent boundary layer was produced for several runs at Mach number 1.9 by a 0.015-inch diameter wire ring installed near the sphere-cone juncture. This change in boundary-layer condition caused a halving of the distance ahead of the jet at which separation occurred, but there was no discernible change in the force or moment due to the jet. Likewise, a three-fold change in Reynolds number had negligible effect.

The moment data presented in Figure 5 can be used to estimate the control characteristics of a hypothetical missile. The results of such an extrapolation are displayed in Figure 9, for a 4.5-foot diameter body of revolution geometrically similar to the model tested. The effects, if any, of Reynolds number and jet gas temperature and specific heat ratio have been neglected. It has been assumed that the non-dimensional interaction effects are equal on model and full-scale body for equal values of the jet force-to-aerodynamic force parameter, $p_{o_j} A^* / p_1 A_1$, where p_{o_j} is the jet stagnation pressure, A* is the nozzle throat area, p_1

is the free stream static pressure, and A_1 is the maximum cross-sectional area of the body.

The moment curves of Figure 9 show a marked non-linearity at the lower Mach numbers. Because of this non-linearity it appears that a given correction in missile heading could be most efficiently obtained by utilizing a large jet force for a short period of time, rather than a small force for a long time. Another effect of the non-linearity is that a small leakage flow from the control jet would produce only a very small moment.

For the design conditions of the hypothetical missile, the effects of jet location and free stream Mach number are crossplotted in Figures 10 and 11. The optimum jet location varies with Mach number, ranging from the most forward position at subsonic speeds to approximately one diameter aft of the nose at supersonic speeds.

The Mach number crossplot (Figure 11) indicates that the adverse interaction effect tends to be most severe in the transonic regime. The data points are not sufficient to determine a minimum value of the specific moment ratio, but they do suggest that it may occur near Mach number 1.4.

Flow Details. Typical schlieren pictures are presented in Figure 12. For all of these pictures except one the jet stagnation pressure was approximately 105 psia. The exception is the picture labeled $p_{o_j}/p_1 = 40$, where the jet pressure was 75 psia. The large variation in free stream static pressure p_1 was obtained by throttling the tunnel inlet, thereby varying the tunnel stagnation pressure, and by changing the Mach number.

Several of the pictures show the model coated with a china clay-oil suspension for the purpose of making visible the line of boundary-layer

separation ahead of the jet. The separation line can be seen in the two upper pictures at Mach number 1.9. Measured locations of the separation line are presented in Figures 13 and 14. These measurements were made either directly from the model after a run or from the schlieren photograph. There was general agreement between the two types of measurement.

The axial pressure distribution thru the jet centerline at Mach number 1.9 is shown in Figure 15, for several different jet stagnation pressures. On each pressure distribution curve the boundary-layer separation point from Figure 13 is indicated.

The circumferential pressure distribution at each of three stations behind the jet is shown in Figure 16. Certain peaks in these distributions are ascribed to either the bow shock, which originates in front of the jet, or to the trailing shock, which begins behind the jet. The locations of these shocks are seen more clearly in the pressure contour plot, Figure 17.

Pressure contours deduced from the axial and circumferential pressure measurements are presented in Figure 17. An approximate integration of these contours indicates an interaction force comparable to the measured interaction force. Since no appreciable effect of the jet is felt on the opposite side of the body at this jet pressure ratio, it appears that the adverse interaction must result from the area of reduced pressures between the bow shock and the trailing shock.

The flow pattern shown in Figure 17 bears so much resemblance to that around a solid cylinder that it might be possible to develope a theory based on this analogy. This theory might consist of an extension of the work of Ferrari (Reference 4) to include the effect of the expansion region between the bow shock and the trailing shock.

CONCLUSION

From the present experimental investigation of a supersonic nose jet issuing perpendicularly into a main stream it is concluded that:

1. Adverse interaction effects are most severe in the transonic regime, reducing the jet effectiveness in an extreme case to one-sixth of its value in a vacuum.
2. For a hypothetical missile the main effects of the adverse interaction are to reduce the available control moment at certain Mach numbers to three-fourths of the vacuum value, and to render the control jet ineffective at low flow rates.
3. The adverse interaction appears to result primarily from a low-pressure region behind the jet, in the area between the jet bow shock and the trailing shock.

It is recommended tha an investigation be initiated to explore the analogy between side-jet flow and the flow around a cylinder projecting perpendicularly from a body. A theory based on this analogy should be capable of describing the adverse interaction effect.

REFERENCES

1. Carvalho, G.F., and Hays, P.B., Jet Interference Experiments Employing Body-Alone and Body-Fin Configurations at Supersonic Speeds, CM-979, The University of Michigan, December 1960.

2. Amick, J.L. and Hays, P.B., Interaction Effects of Side Jets Issuing from Flat Plates and Cylinders Alined with a Supersonic Stream, WADD TR 60-329, Wright Air Development Division, June 1960.

3. Amick, J.L. and Carvalho, G.F., Interaction Effects of a Jet Flap on a 60° Delta Wing at Mach Number 4, and Comparison with Two-dimensional Theory, CM-1031, The University of Michigan, February 1963.

4. Ferrari, Carlo, Interference between a Jet Issuing Laterally from a Body and the Enveloping Supersonic Stream, BB Report 286, The Johns Hopkins University Applied Physics Laboratory, April 1959.

APPENDIX A

ESTIMATED SPECIFIC IMPULSE IN VACUUM

The normal force of the jet in a vacuum is merely the sum of the vertical components of pressure force acting on all the surfaces of the nozzle. By reference to Figure 3 this can be written

$$N_{vac} = \pi r_1^2 p_b + \int_{abc} p \cos\phi \, dS + \int_{defgh} p \cos\phi \, dS \qquad (A1)$$

where πr_1^2 is the area of the base of the plug, p_b is the base pressure, ϕ is the angle between the normal to the surface and the vertical, and the integrals are taken over the interior surfaces of the plug and the nozzle cavity, respectively.

Another expression for the value of these integrals is obtained from the momentum theorem, which states that for steady flow the sum of the vertical components of pressure force acting on a control surface is equal to the flux of vertical momentum thru that surface. The control surface shown in Figure 3 includes a toroidal portion $\widehat{ad}$ along which the flow properties, designated by primes, are assumed to be constant. (This is equivalent to the radial-flow assumption in a conical nozzle.) For this control surface the momentum theorem gives

$$p' \int_{ad} \cos\phi \, dA' + \int_{abc} p \cos\phi \, dS + \int_{defgh} p \cos\phi \, dS = - \rho'(V')^2 \int_{ad} \cos\phi \, dA' \qquad (A2)$$

Since $\cos\phi = - \cos\theta$, $\cos\phi \, dA' = - dA$, where dA is the projection of the element of toroidal area dA' on the plane of the base of the plug. Then (A2) becomes

$$\int_{abc} p \cos\phi \, dS + \int_{defgh} p \cos\phi \, dS = \left[p' + \rho'(V')^2 \right] A \qquad (A3)$$

where A is the nozzle exit area in the plane of the base of the plug.

Equations (A1) and (A3) combine to give

$$N_{vac} = \left[p' + \rho' (V')^2 \right] A + \pi r_1^2 p_b = p' A \left[1 + \gamma (M')^2 \right] + \pi r_1^2 p_b \tag{A4}$$

The flow rate, in terms of pounds mass per second, can be written

$$\dot{m} = g \rho' A' V' = \frac{g \gamma p' A' M'}{a'} = \frac{g \gamma p' A' M'}{a_{o_j} (a'/a_{o_j})} \tag{A5}$$

The specific impulse is then obtained by dividing (A4) by (A5)

$$I_{s_{vac}} = \frac{N_{vac}}{\dot{m}} = a_{o_j} \frac{a'}{a_{o_j}} \frac{A}{A'} \frac{\left[1 + \gamma (M')^2 + \frac{p_b}{p'} \frac{r_1^2}{r_2^2 - r_1^2} \right]}{g \gamma M'} \tag{A6}$$

The area A' of the toroidal surface is, by integration of the element of area in Figure 3,

$$A' = \int_0^{\theta_1} 2\pi (r_2 - R \sin\theta) \, R d\theta = 2\pi R \left[r_2 \theta_1 + R (\cos\theta_1 - 1) \right]$$

But $R = \frac{r_2 - r_1}{\sin\theta_1}$, so that $A' = 2\pi (r_2 - r_1) \left[\frac{r_2 \theta_1}{\sin\theta_1} - \frac{r_2 - r_1}{1 + \cos\theta_1} \right]$ (A7)

This can be approximated very well by

$$\frac{A'}{A} = 1 + \theta_1^2 \frac{\left(1 - \frac{\theta_1^2}{30} + \cdots \right) r_2 + \left(3 + \frac{\theta_1^2}{2} + \cdots \right) r_1}{12 (r_2 + r_1)} \tag{A8}$$

The quantities M' and a'/a_{o_j} in equation (A8) are found from isentropic flow relations as functions of the area ratio A'/A^*, where A^* is the throat area of the nozzle.

For the plug nozzle of the present tests

$A^* = .001665$ sq. in.

$A = .01022$ sq. in.

$\theta_1 = 15^\circ$

$r_1 = .0300$ in.

$r_2 = .06445$ in.

$\gamma = 1.4$

$a_{o_j} = 1127$ ft. per sec.

$g = 32.2$ ft. per sec^2.

Then $A' = 1.009394$

$A = .01032$ sq. in.

$A'/A^* = 6.201$

$M' = 3.403$

$a'/a_{o_j} = .5495$

The specific impulse is, assuming $\frac{p_b}{p'} = 1/3$,

$I_{s_{vac}} = 69.2$ secs

The base pressure ratio has only a weak effect on specific impulse. Increasing the base pressure to $p_b = p'$ would only increase $I_{s_{vac}}$ by about one percent.

APPENDIX B

AMBIENT PRESSURE EFFECT

The ambient pressure into which a jet discharges reduces the net force of the jet, compared with the force it would produce in a vacuum. For a jet nozzle with a large expansion ratio, as in the present case, the effect can be quite large.

A theoretical estimate of the ambient pressure effect can be obtained from momentum considerations, with the following assumptions:

1. Boundary-layer effects on the mass flow and thrust are neglected,
2. Separation inside the nozzle due to high ambient pressure is neglected, and
3. Flow induced by the jet is neglected.

When the jet is operating, the normal force due to pressures acting on the inside surfaces of the nozzle and on the end of the plug is (see Appendix A)

$$N_{vac} = \left[1 + \gamma (M')^2\right] p' A + p_b A_b \tag{B1}$$

where A_b is the area of the end of the plug ($= \pi r_1^2$). When the jet is off, the force due to pressures acting on these same surfaces is

$$N_o = p_a (A + A_b) \tag{B2}$$

where p_a is the ambient pressure. The net force due to the jet is therefore

$$N = N_{vac} - N_o = N_{vac} - p_a (A + A_b) \tag{B3}$$

The specific impulse of this net force is obtained by dividing (B3) by $\dot{m}$,

$$I_s = I_{s_{vac}} - \frac{p_a (A + A_b)}{\dot{m}} \tag{B4}$$

Rearranging (B4) gives

$$I_{s_{vac}} = I_s + \frac{p_a (A + A_b)}{\dot{m}} \tag{B5}$$

The specific impulse in a vacuum can thus be estimated from experimental data obtained with the jet discharging into an ambient pressure p_a, by means of equation (B5).

The specific impulse ratio is found by dividing (B3) by (B1)

$$\frac{I_s}{I_{s_{vac}}} = 1 - \frac{p_a \left[1 + \frac{\gamma - 1}{2} (M')^2\right]^{\frac{\gamma}{\gamma - 1}}}{p_{o_j} \left[\left(1 + \gamma (M')^2\right) \frac{A}{(A + A_b)} \frac{p_b}{p'} \frac{A_b}{(A + A_b)}\right]} \tag{B6}$$

For $M' = 3.403$, $p_b / p' = 1/3$, $\frac{A_b}{A + A_b} = .217$, $\gamma = 1.4$

$$\frac{I_s}{I_{s_{vac}}} = 1 - \frac{p_a}{p_{o_j}} \frac{66.38}{17.21\ (.783) + .333\ (.217)}$$

$$= 1 - \frac{p_a}{p_{o_j}} \frac{66.38}{13.46 + .07}$$

$$= 1 - 4.94 \frac{p_a}{p_{o_j}} \tag{B7}$$

The specific moment ratio follows from the above as

$$\frac{M_s}{M_{s_{vac}}} = \frac{I_s\ (5.31 - j)}{I_{s_{vac}}\ 4.91} \tag{B8}$$

where j is the distance to the jet from the nose, divided by the maximum body diameter.

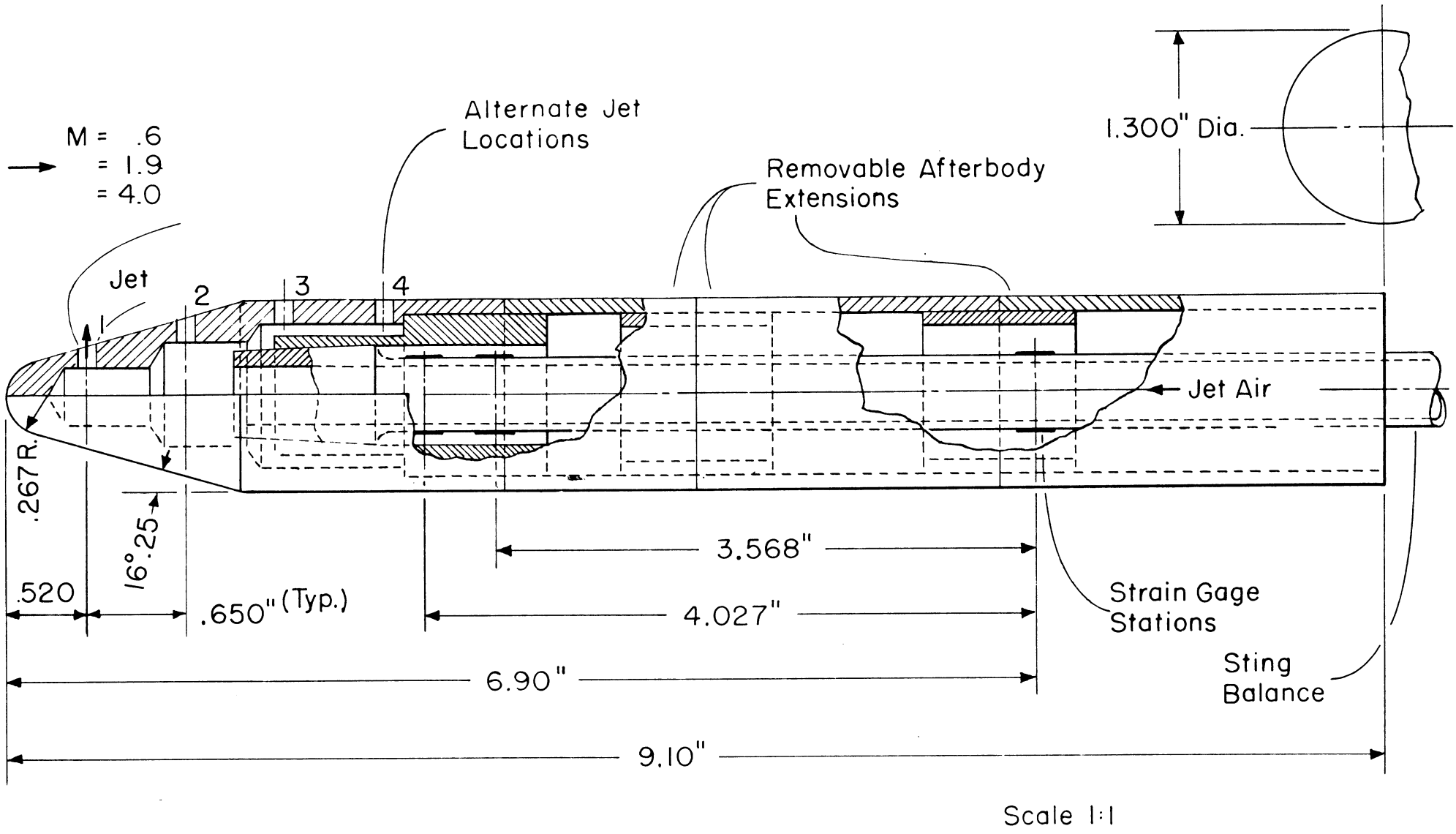

FIGURE 1. GENERAL ARRANGEMENT OF MODEL.

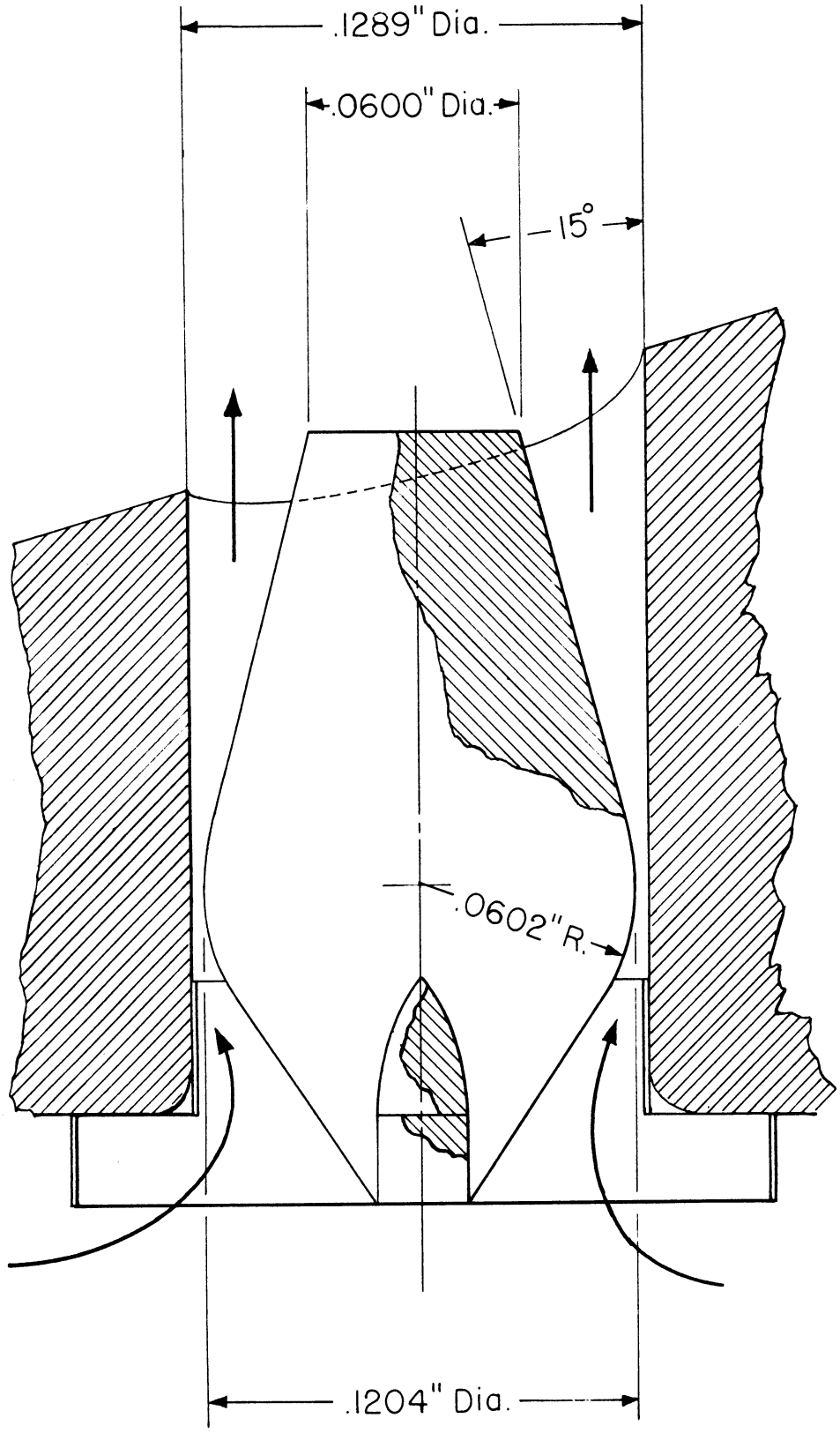

Scale 20:1

FIGURE 2. PLUG NOZZLE DETAILS.

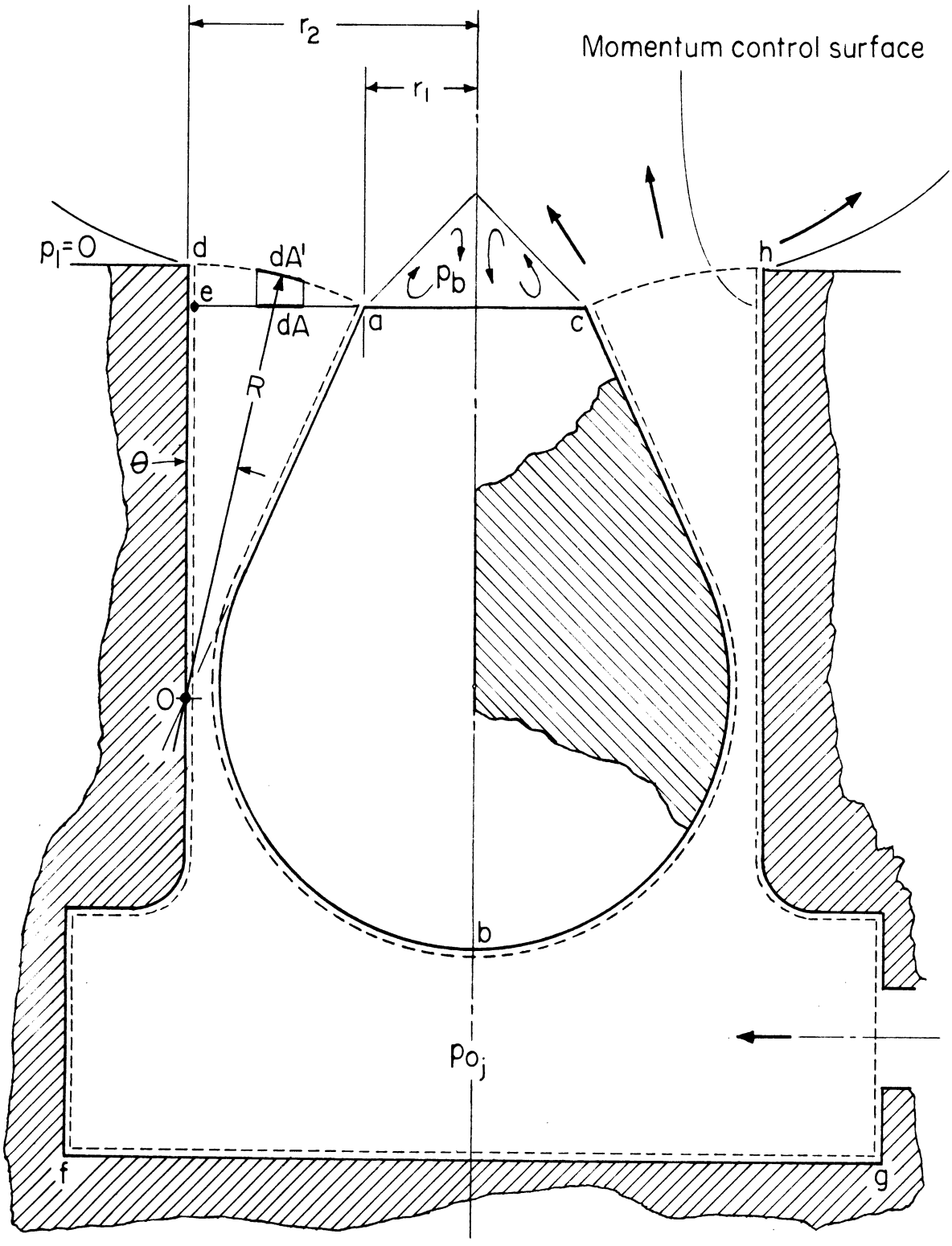

FIGURE 3. ANALYSIS OF PLUG NOZZLE FLOW INTO A VACUUM.

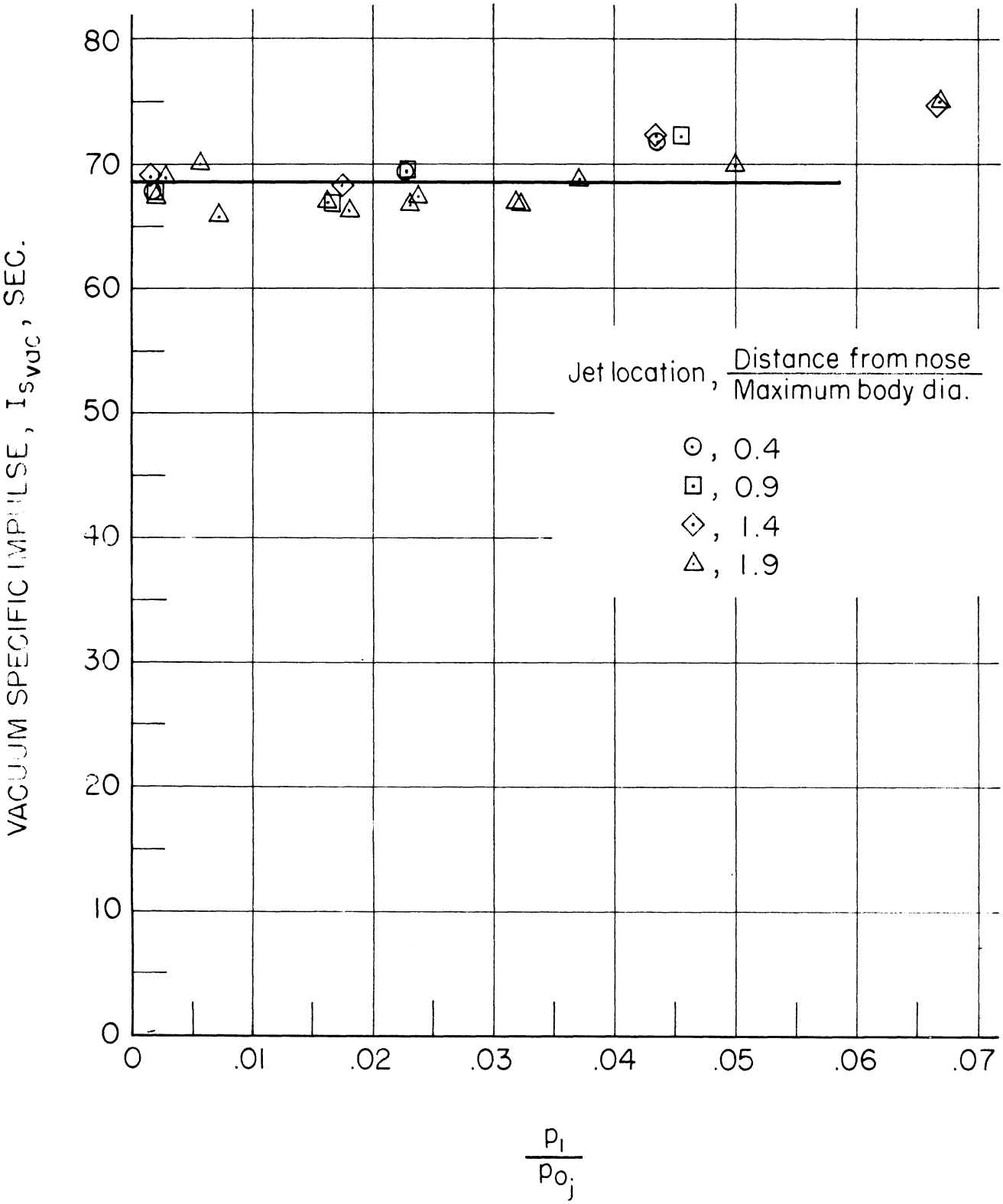

FIGURE 4. INDICATED SPECIFIC IMPULSE IN VACUUM FROM EXPERIMENTAL DATA CORRECTED FOR AMBIENT PRESSURE EFFECT.

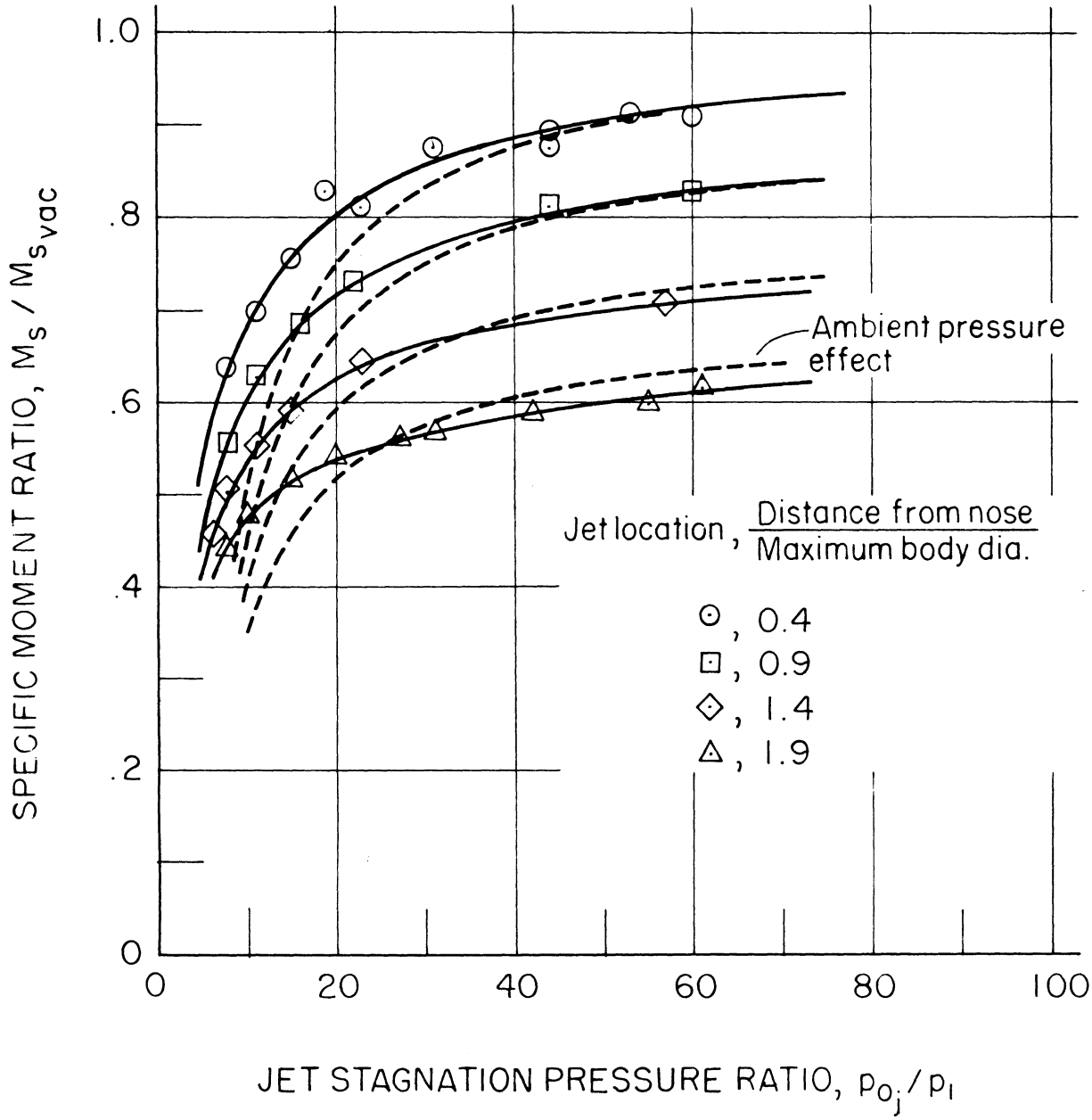

(a) M = 0

FIGURE 5. SPECIFIC MOMENT RATIO AT ZERO ANGLE OF ATTACK, FOR VARIOUS JET LOCATIONS AND MACH NUMBERS.

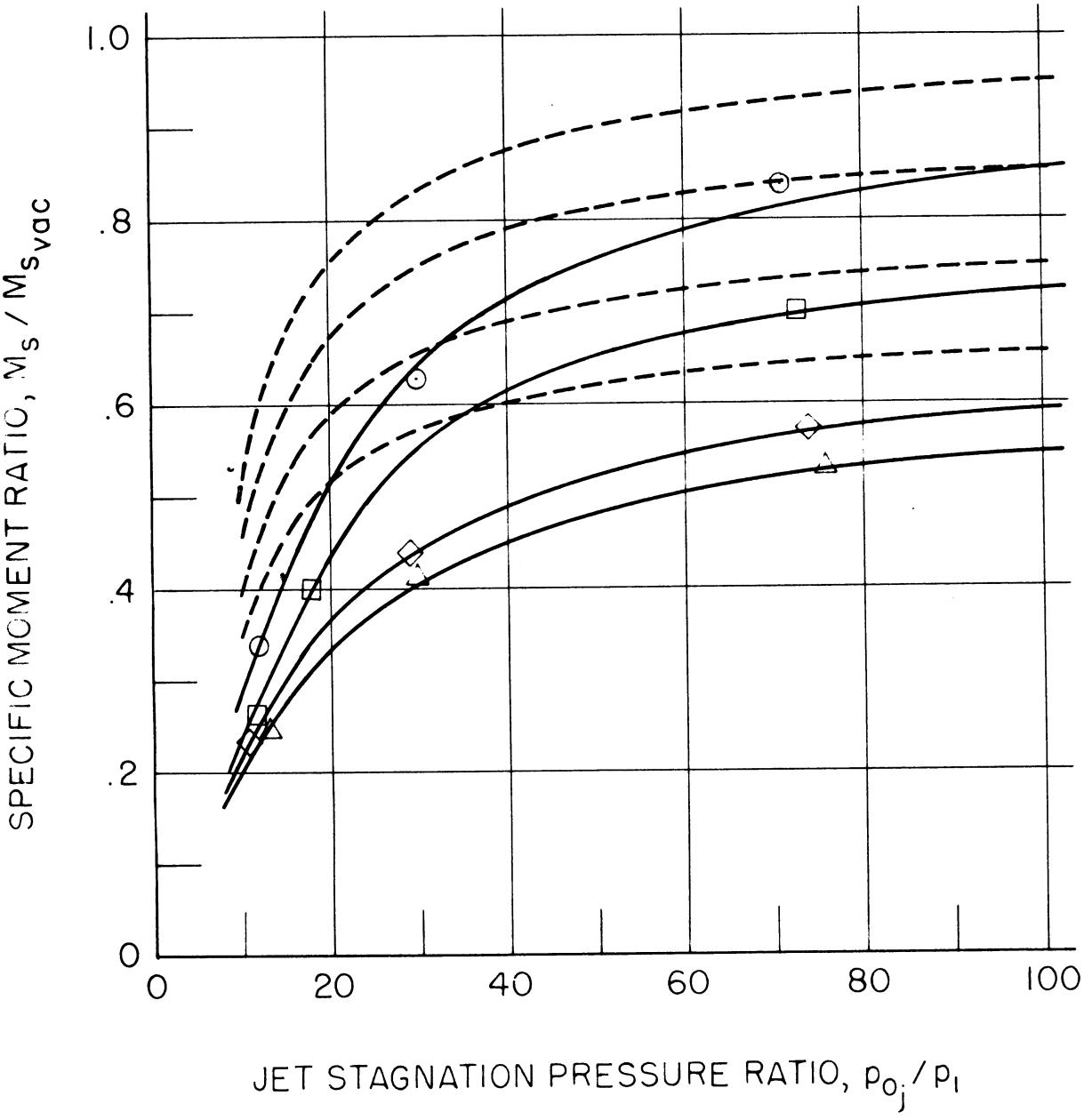

(b) M = 0.6

FIGURE 5. Continued.

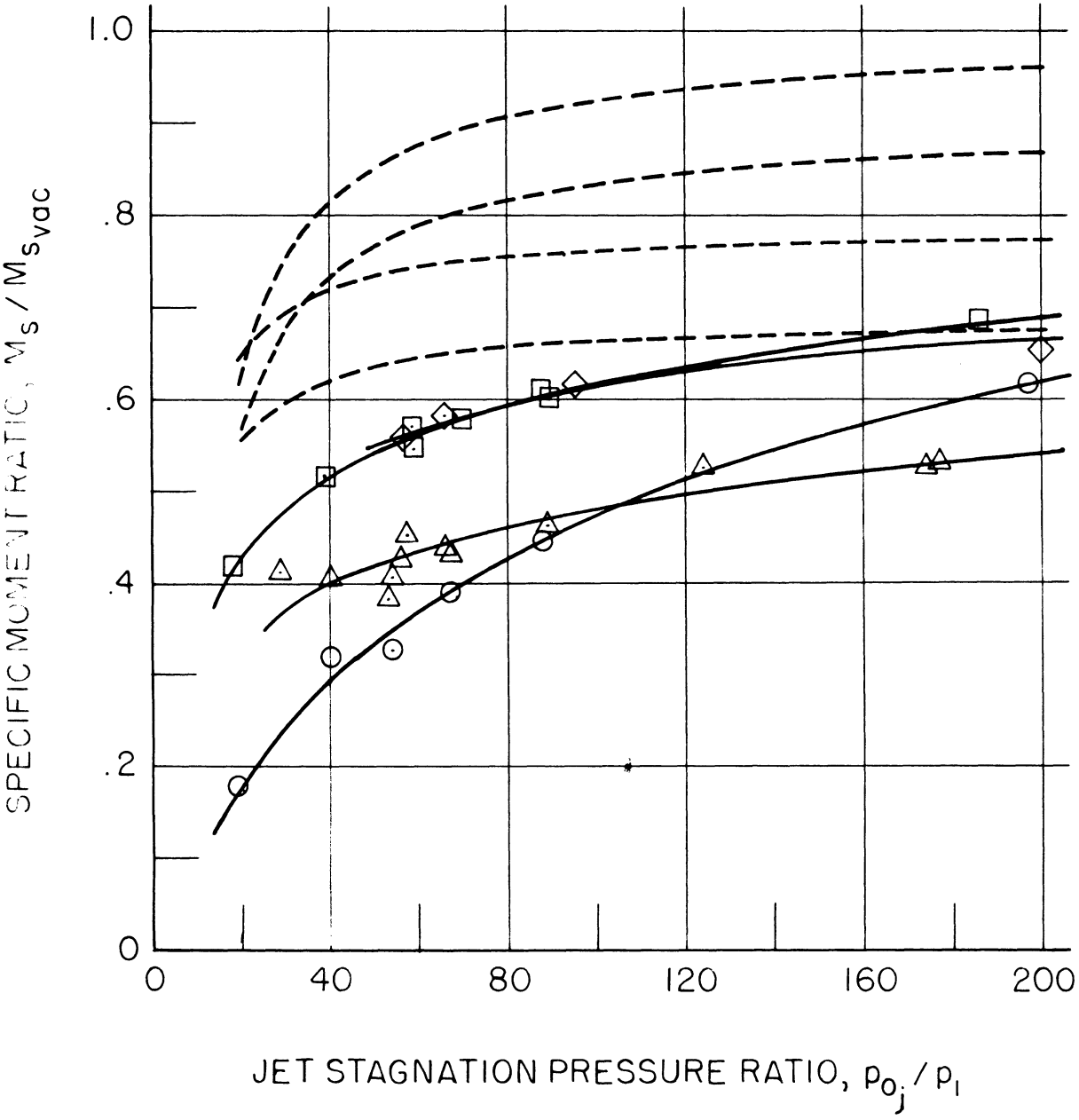

(c) M = 1.9

FIGURE 5. Continued.

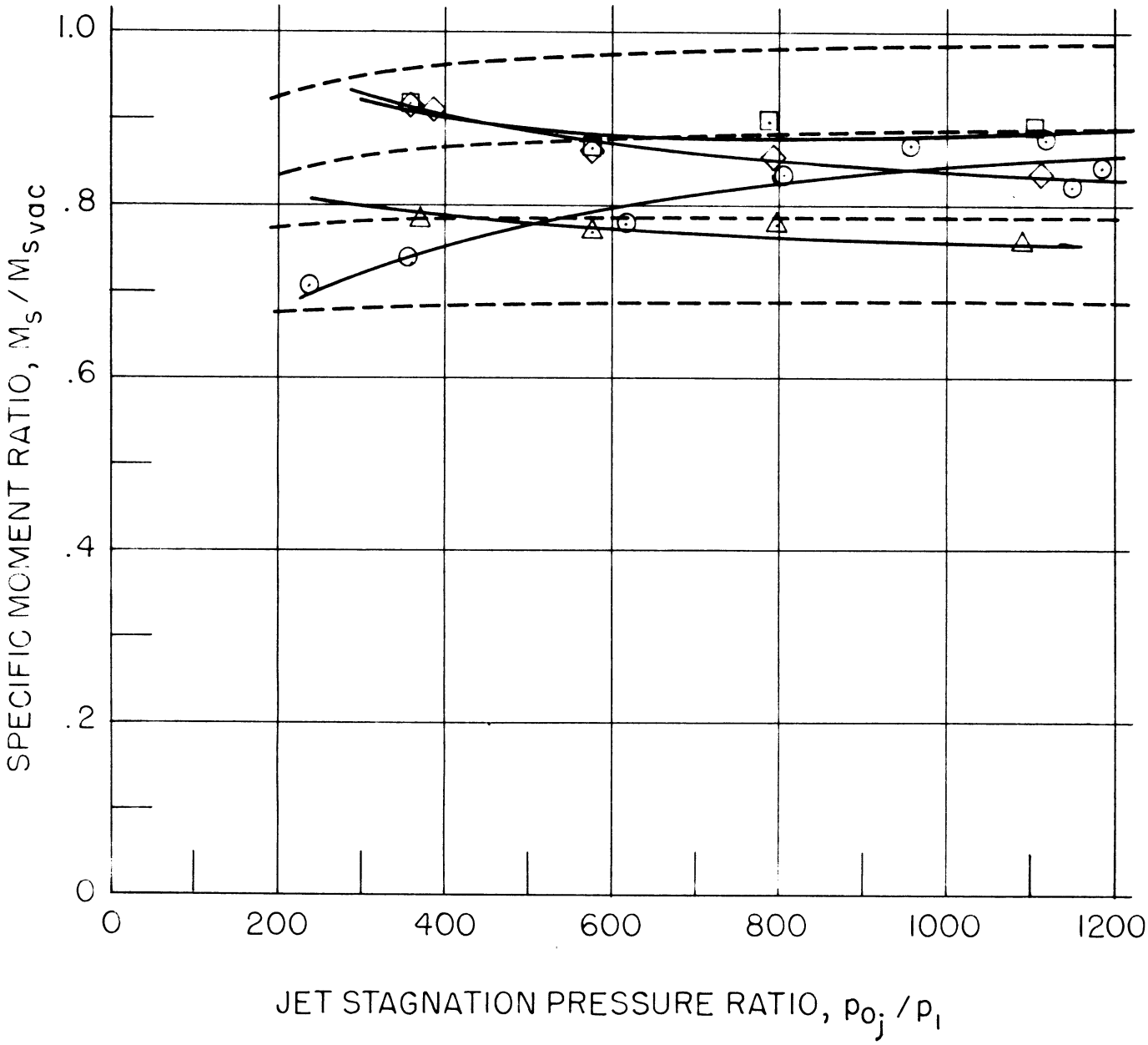

(d) M = 4.0

FIGURE 5. Concluded.

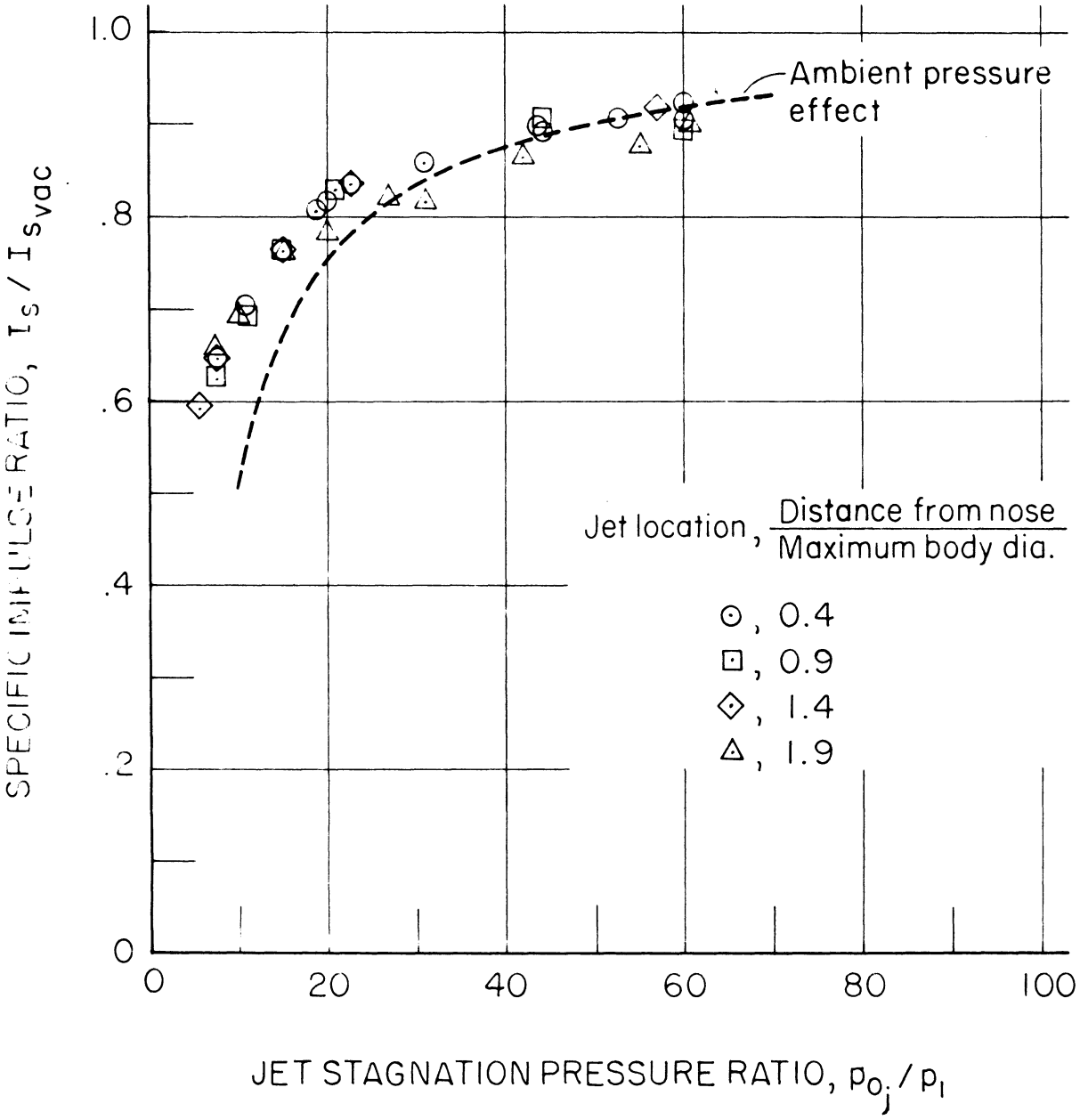

(a) M = 0

FIGURE 6. SPECIFIC IMPULSE RATIO AT ZERO ANGLE OF ATTACK, FOR VARIOUS JET LOCATIONS AND MACH NUMBERS.

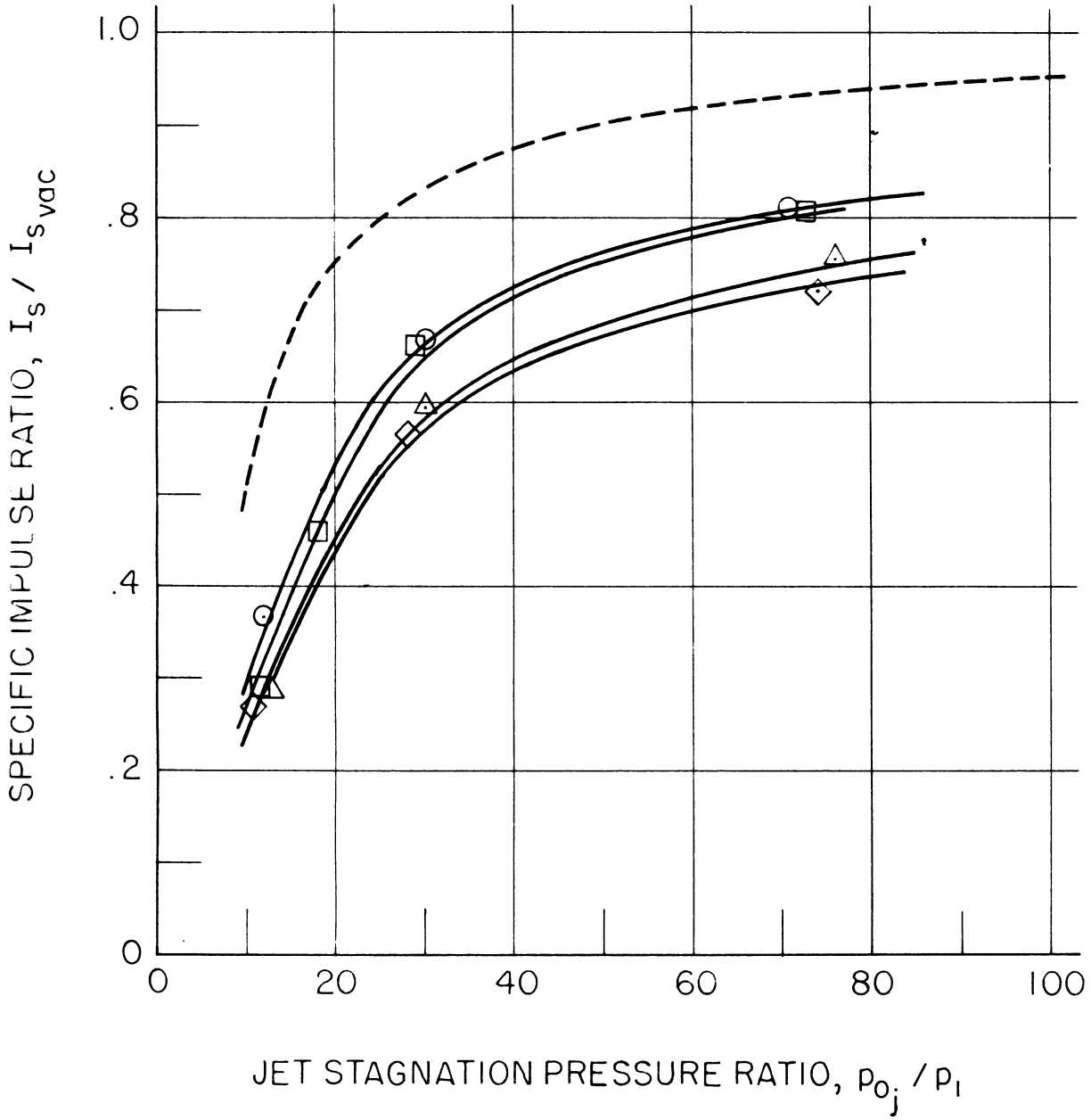

(b) M = 0.6

FIGURE 6. Continued.

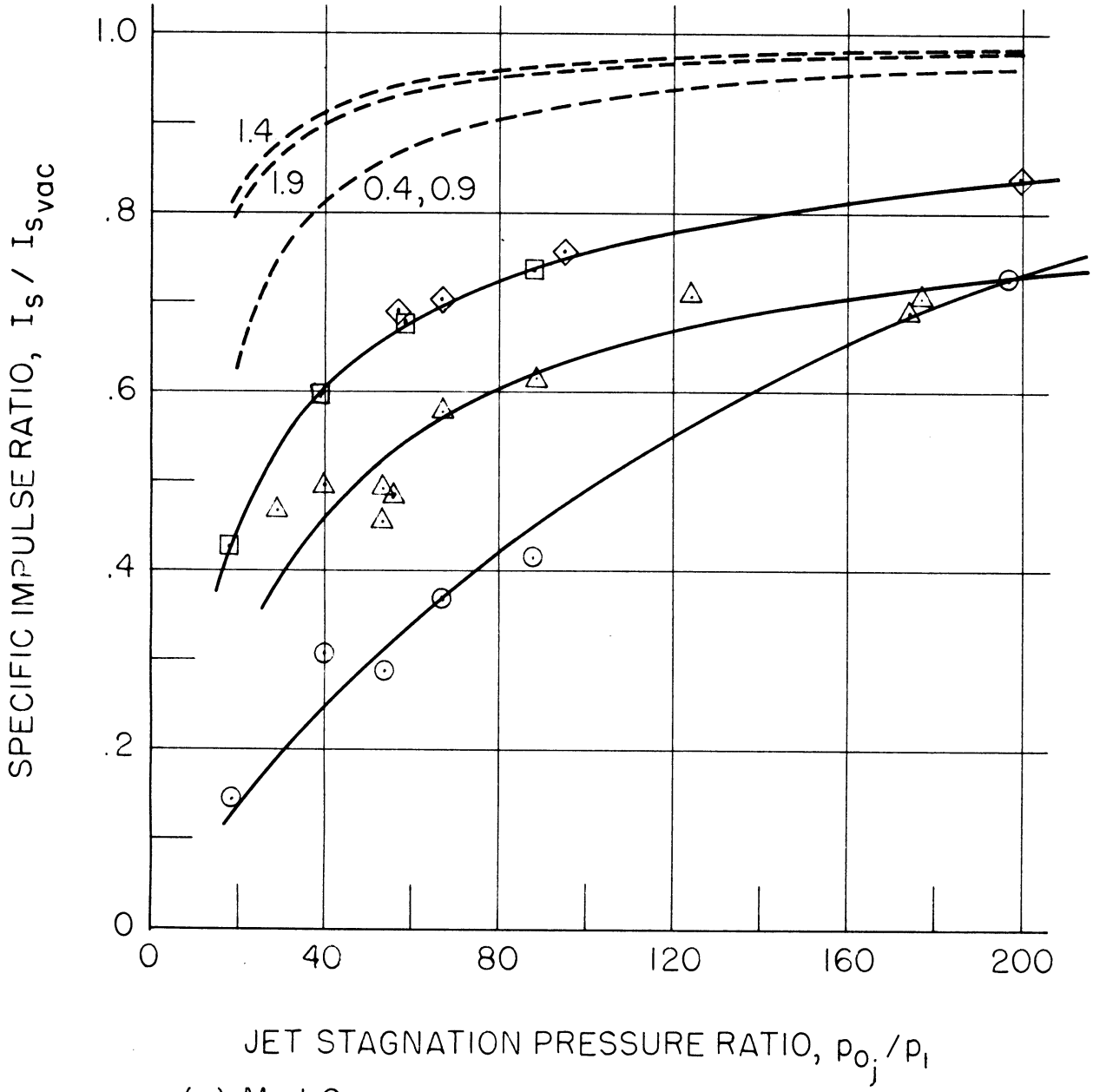

(c) M = 1.9

FIGURE 6. Continued.

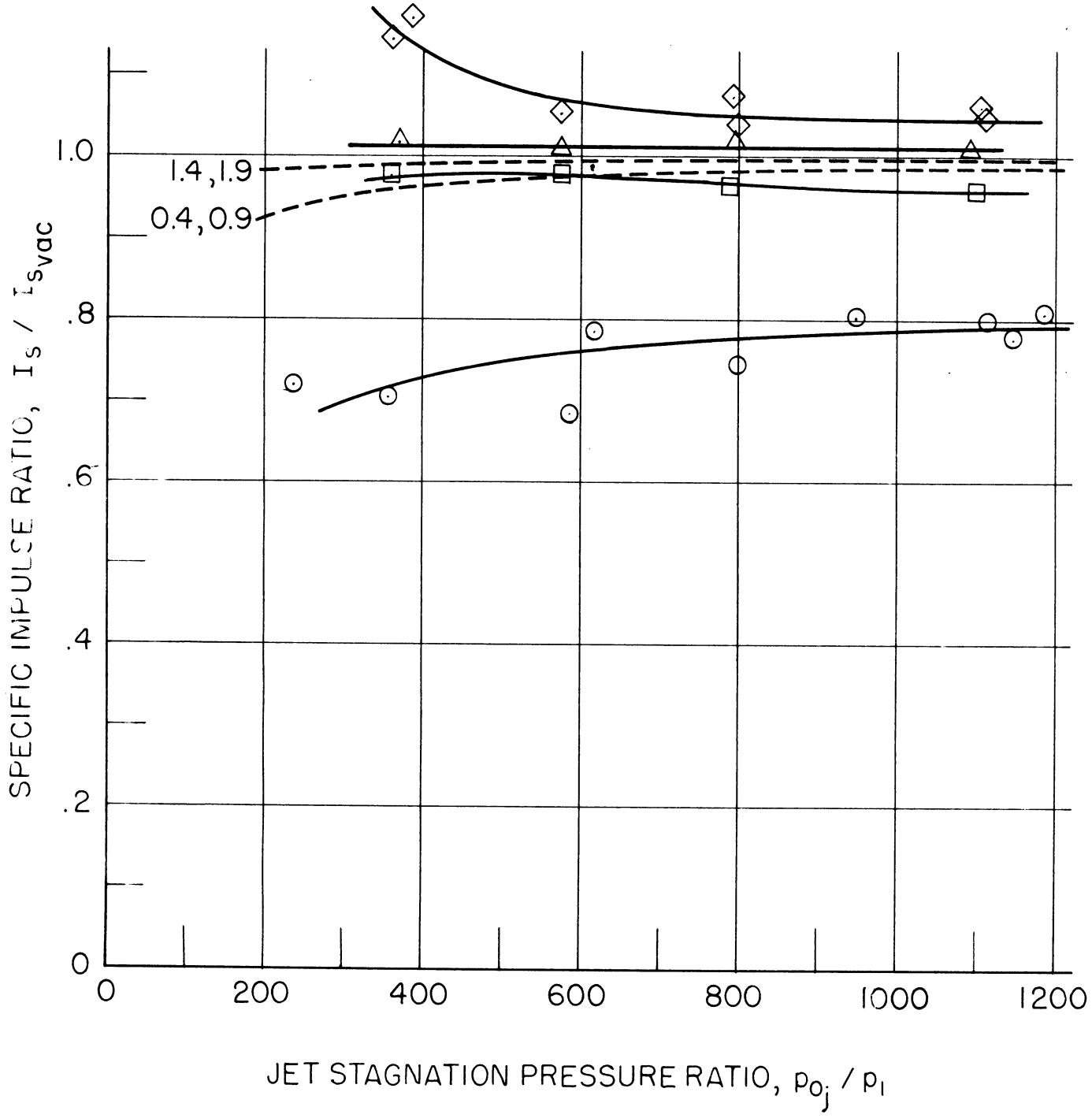

(d) M = 4.0

FIGURE 6. Concluded.

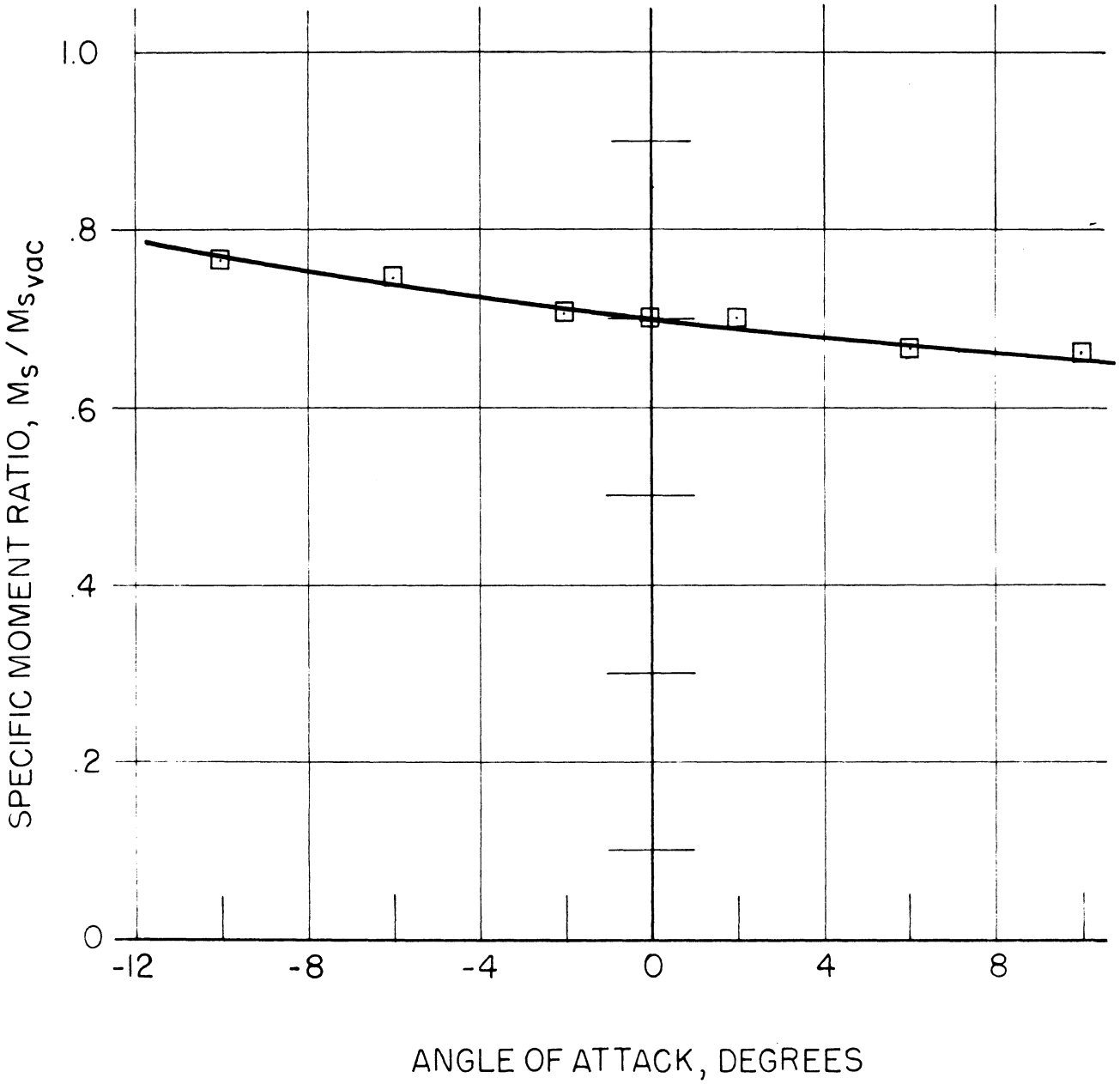

(a) $M = 0.6$, $\frac{p_{0_j}}{p_1} = 75$

Jet location, $\frac{\text{Distance from nose}}{\text{Maximum body dia.}}$

⊡, 0.9

FIGURE 7. EFFECTS OF ANGLE OF ATTACK ON SPECIFIC MOMENT RATIO.

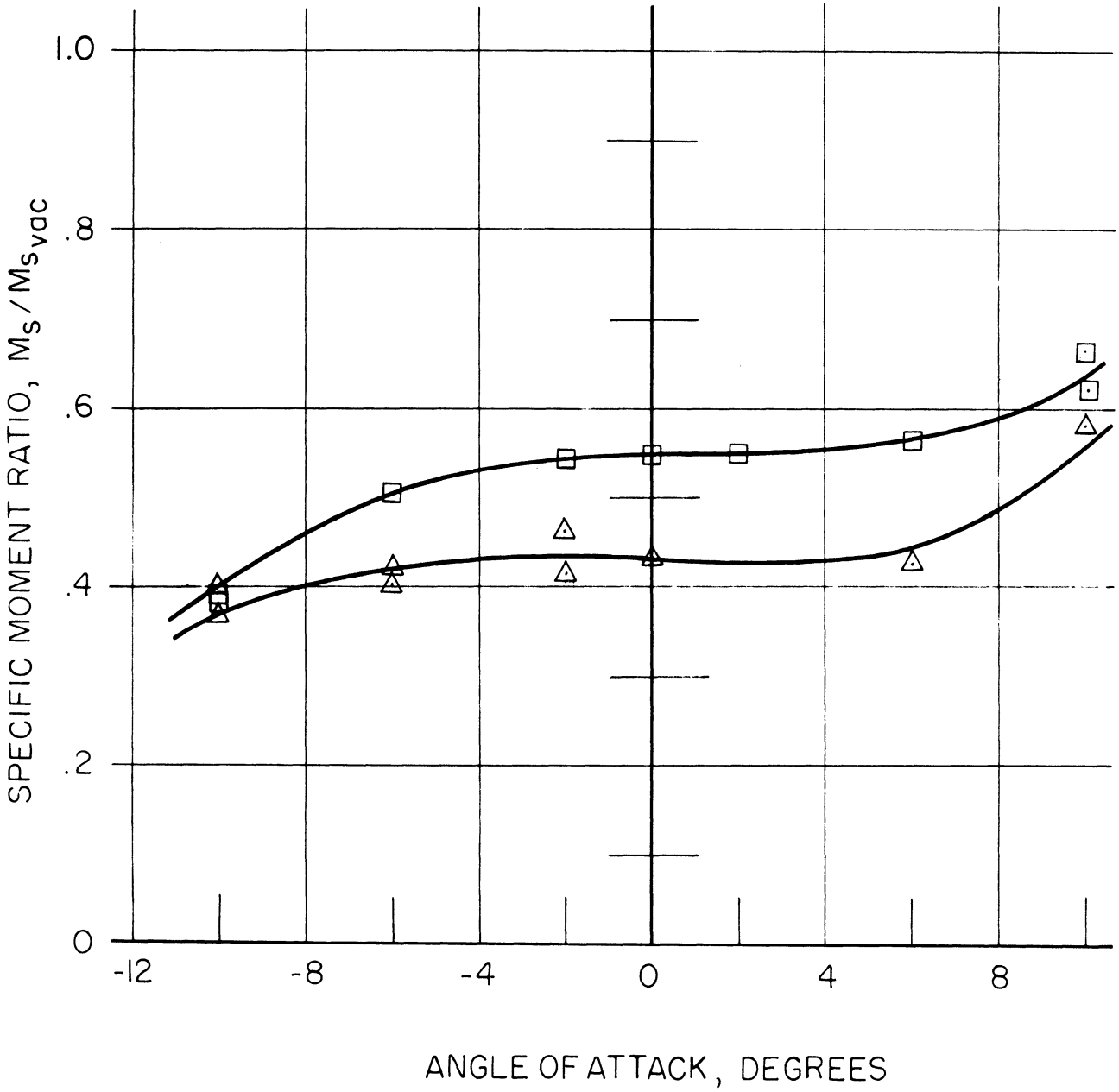

(b) $M = 1.9$, $\frac{p_{0_j}}{p_l} = 55$

□ 0.9
△ 1.9

FIGURE 7. Continued.

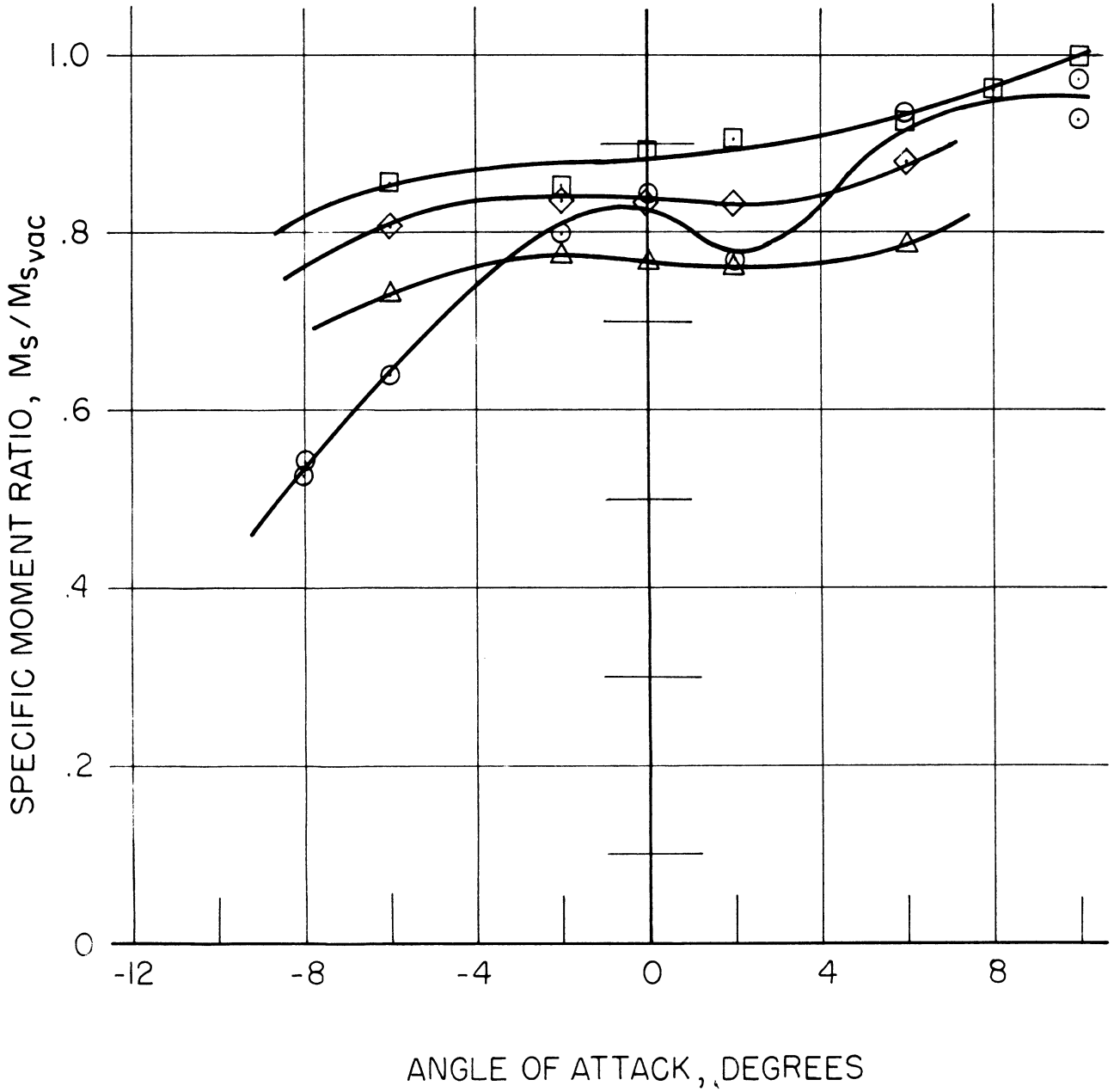

(c) M = 4.0, $\frac{p_{0_j}}{p_l} = 1150$

⊙	0.4
⊡	0.9
◇	1.4
△	1.9

FIGURE 7. Concluded.

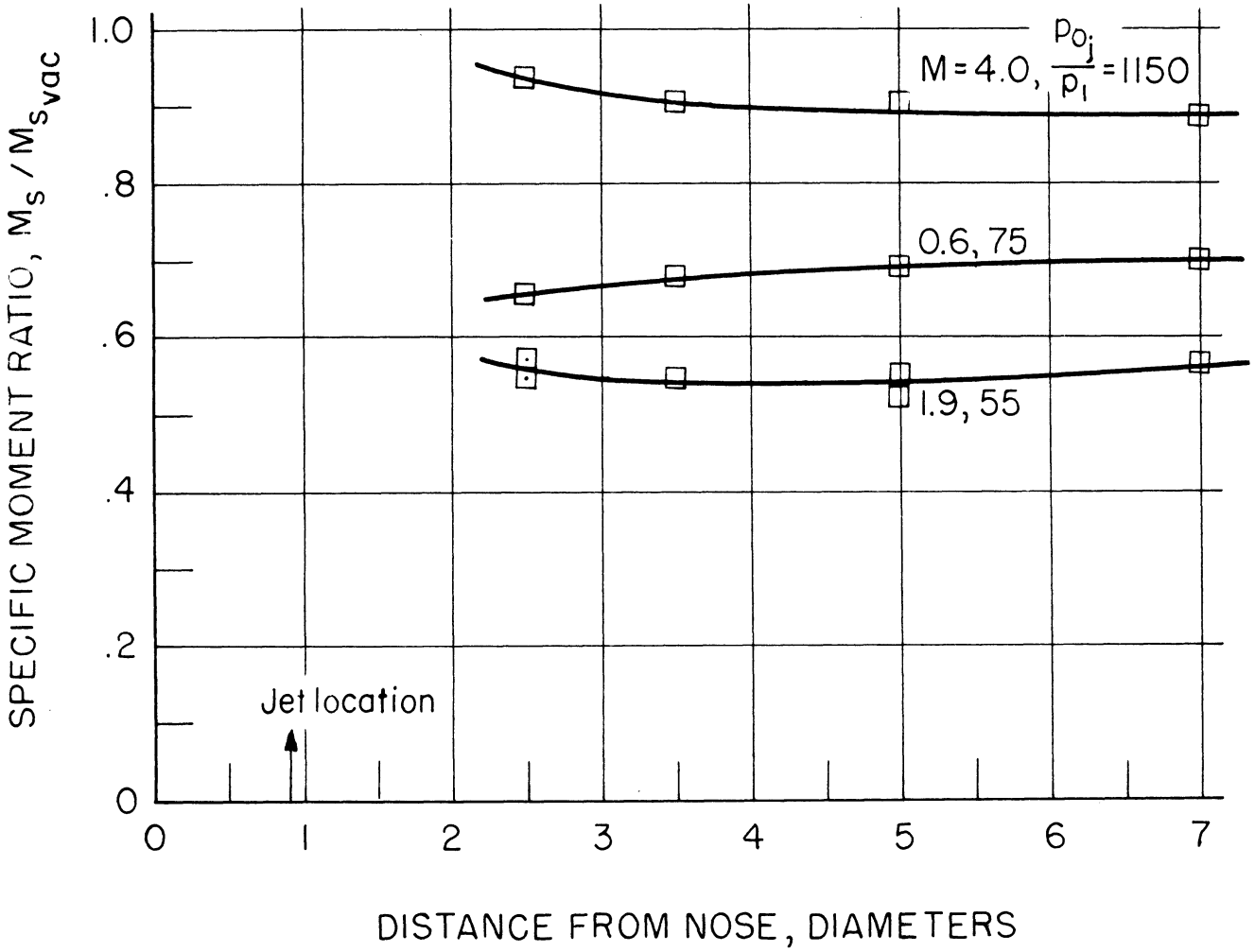

FIGURE 8. EFFECTS OF BODY LENGTH ON SPECIFIC MOMENT RATIO AT ZERO ANGLE OF ATTACK. JET LOCATION 0.9 BODY DIAMETERS AFT OF NOSE .

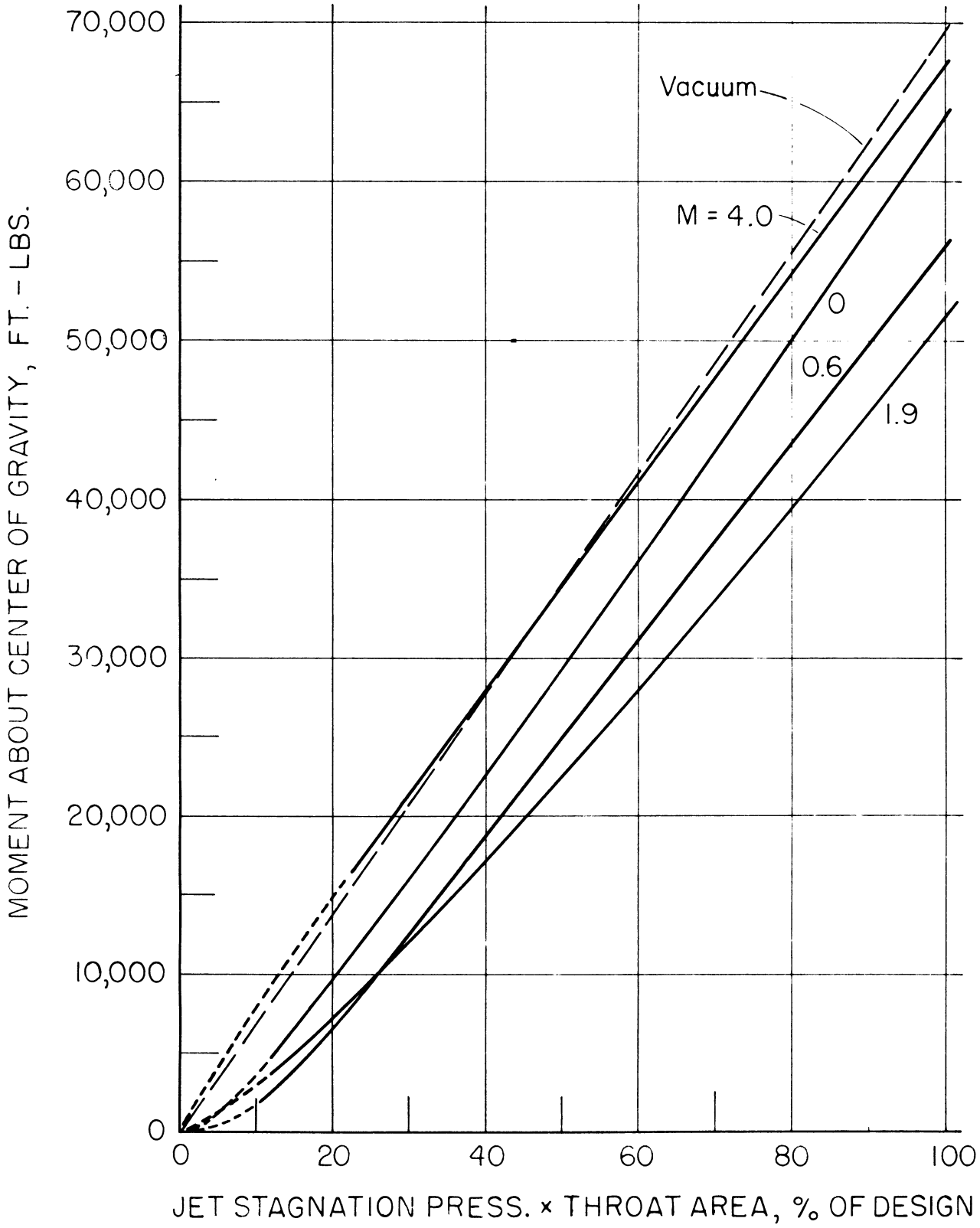

(a) Jet location = 0.9 dia. aft of nose

FIGURE 9. PREDICTED MOMENTS OF CONTROL JET ABOUT A CENTER OF GRAVITY POSITION 5.31 DIAMETERS AFT OF NOSE. BODY DIAMETER = 4.5 FT.; ALTITUDE = SEA LEVEL AT M = 0; 15,000 FT. AT M = 0.6; 25,000 FT. AT M = 1.9; AND 64,000 FT. AT M = 4.0. $\alpha = 0$.

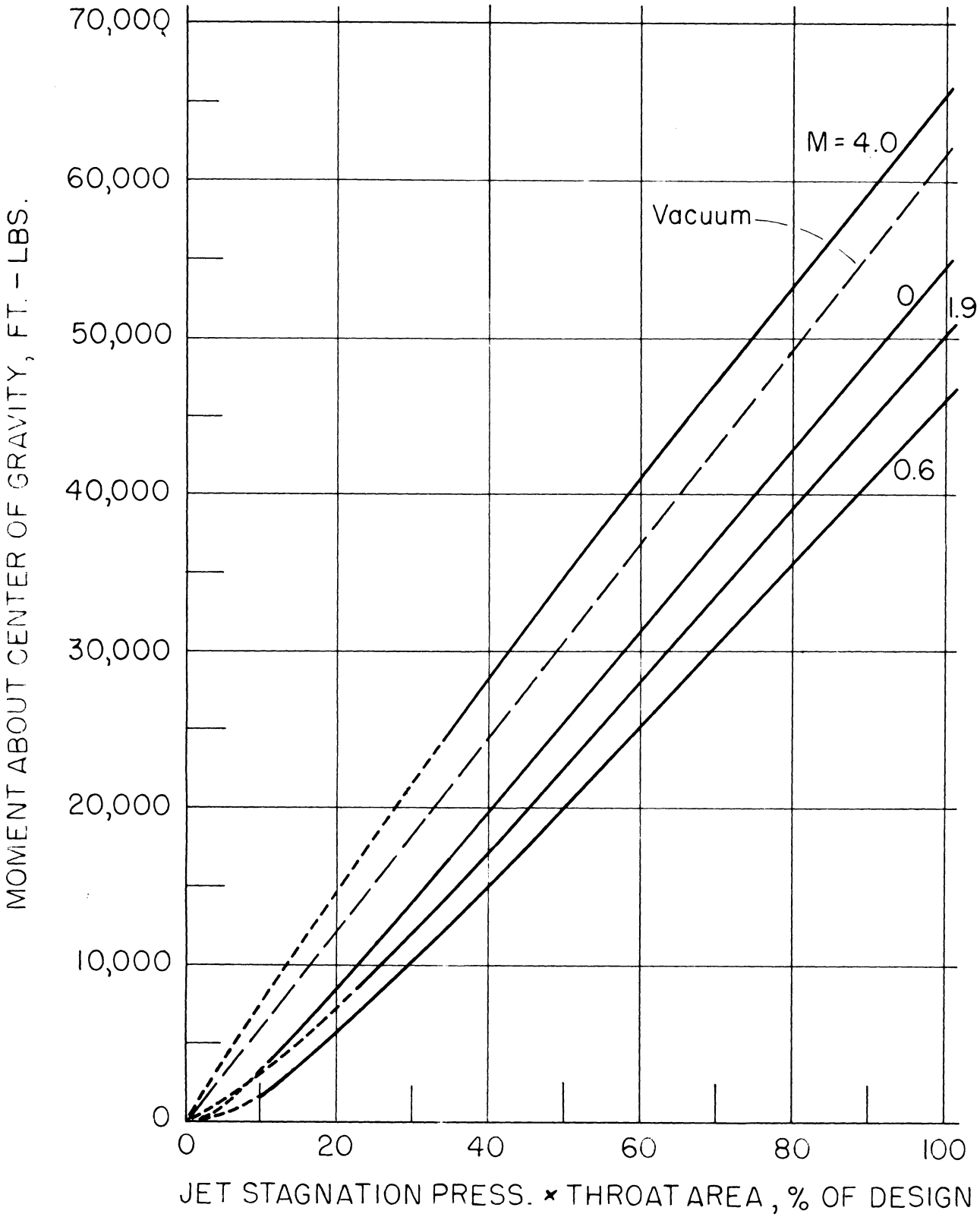

(b) Jet location = 1.4 dia. aft of nose

FIGURE 9. Concluded.

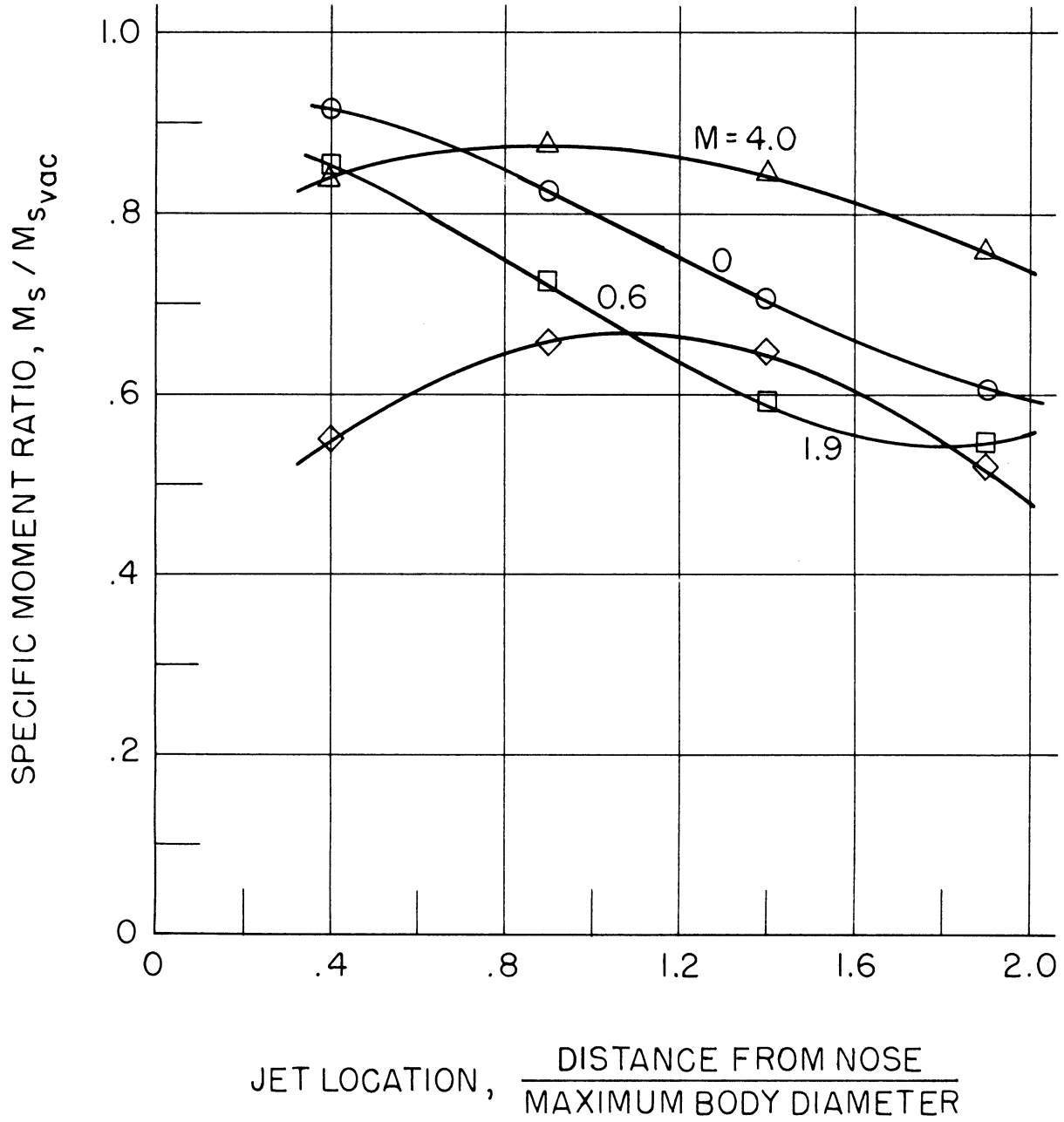

FIGURE 10. EFFECT OF JET LOCATION ON SPECIFIC MOMENT RATIO AT THE DESIGN CONDITIONS OF FIGURE 9.

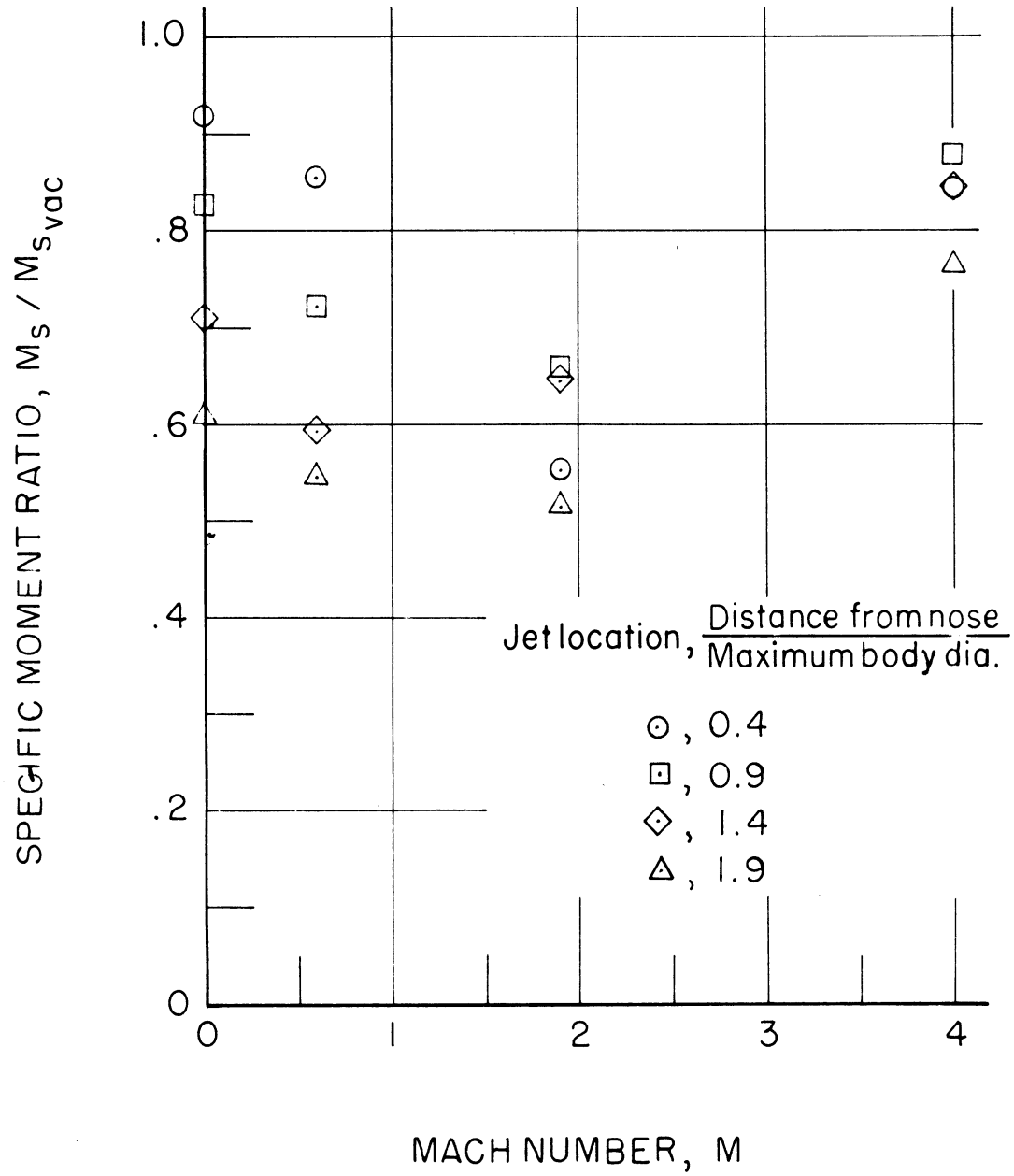

FIGURE 11. EFFECT OF MACH NUMBER ON SPECIFIC MOMENT RATIO AT THE DESIGN CONDITIONS OF FIGURE 9.

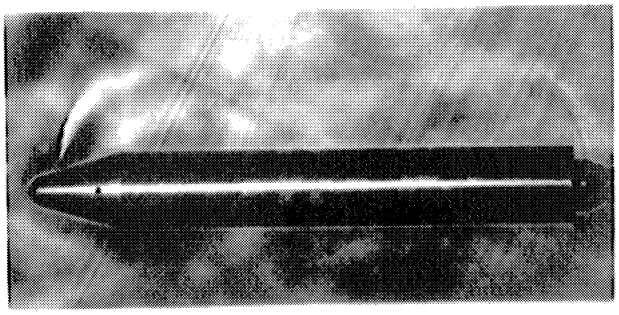

$p_{0_j}/p_1 = 71$

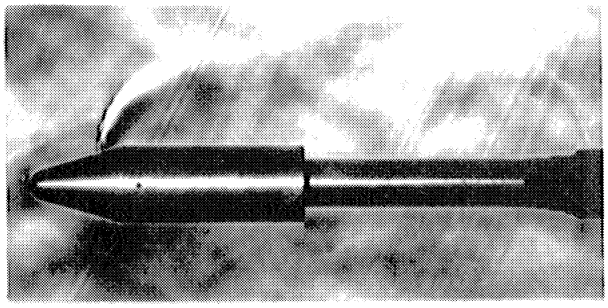

$p_{0_j}/p_1 = 72$

M = 0.6

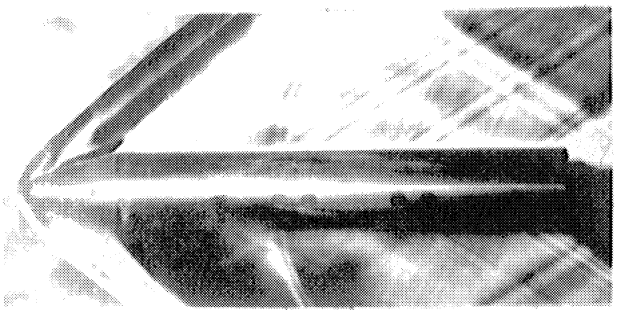

$p_{0_j}/p_1 = 40$

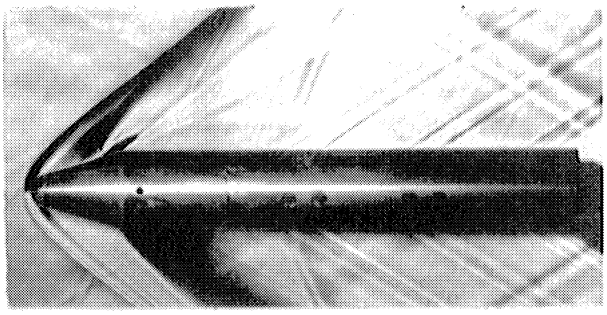

$p_{0_j}/p_1 = 59$

M = 1.9

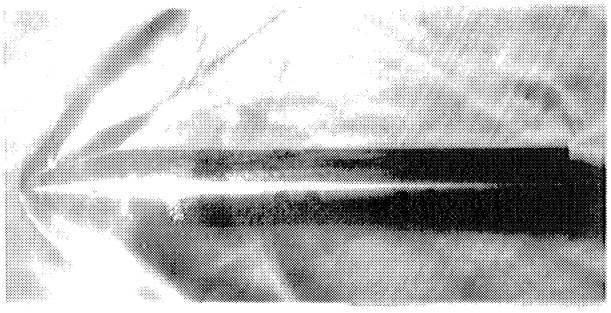

$p_{0_j}/p_1 = 197$

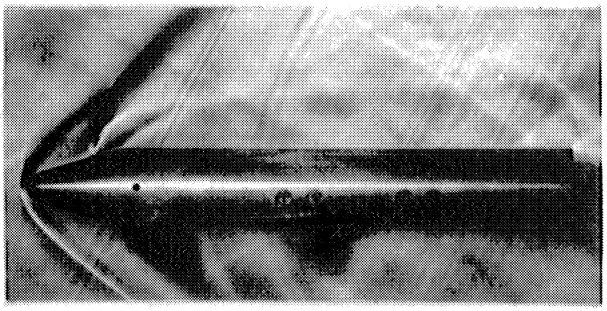

$p_{0_j}/p_1 = 190$

M = 1.9

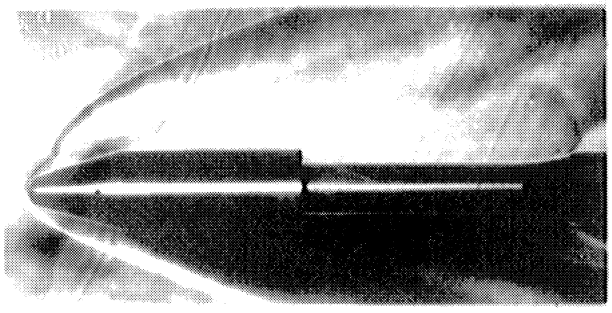

$p_{0_j}/p_1 = 1149$

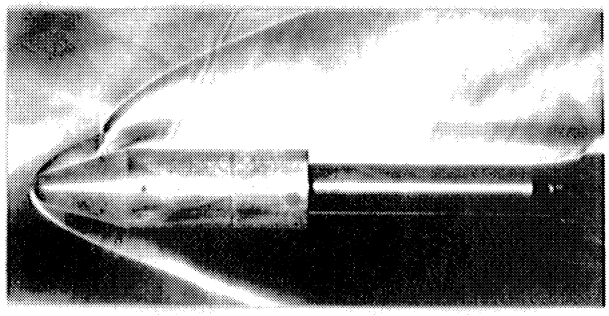

$p_{0_j}/p_1 = 1116$

M = 4.0

FIGURE 12 TYPICAL SCHLIEREN PICTURES. JET LOCATION 0.4 OR 0.9 DIAMETERS FROM NOSE. $\alpha = 0$.

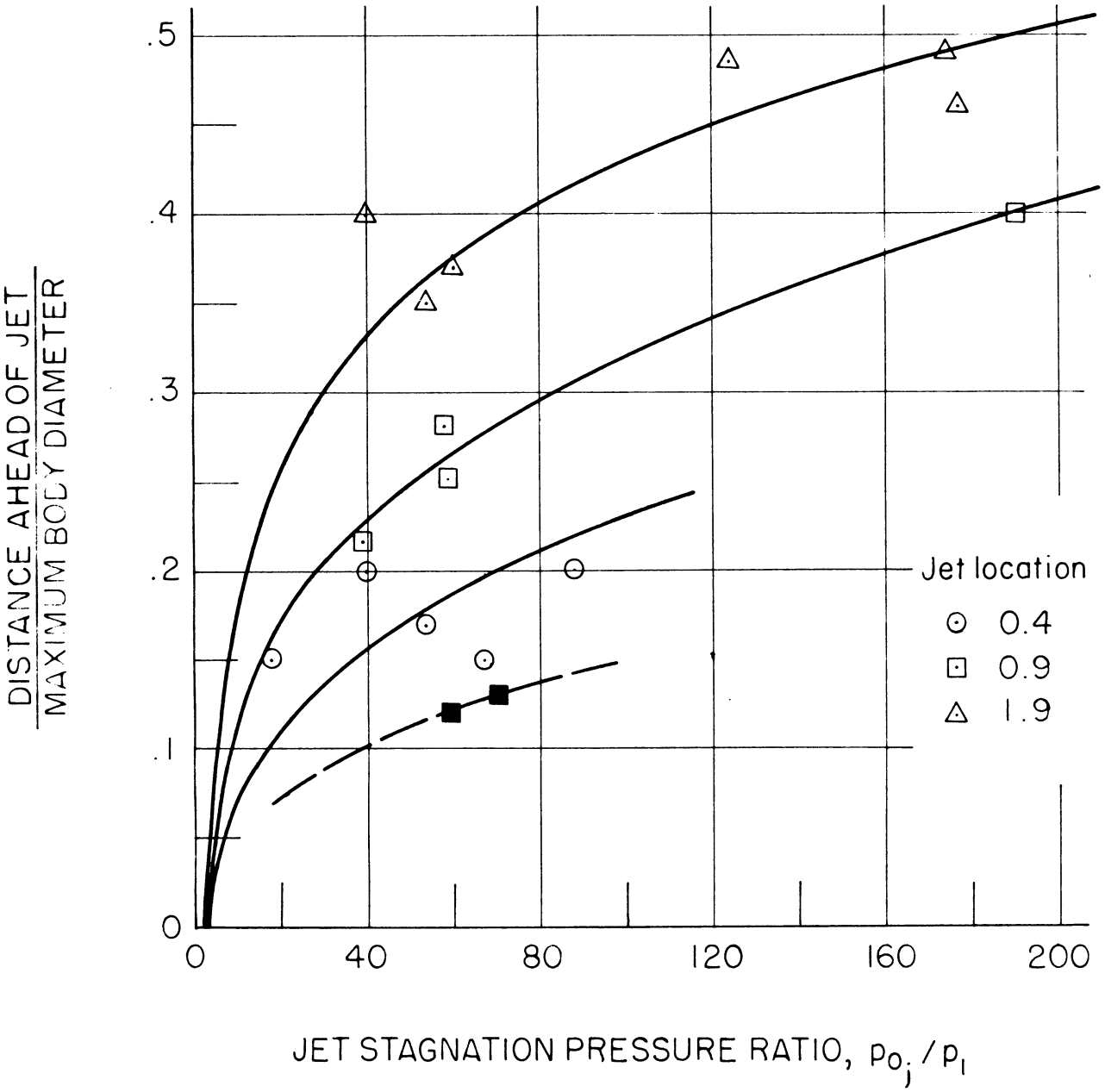

FIGURE 13. LOCATION OF LINE OF BOUNDARY-LAYER SEPARATION. SOLID SYMBOLS INDICATE TURBULENT BOUNDARY LAYER.
$M = 1.9$, $\alpha = 0$.

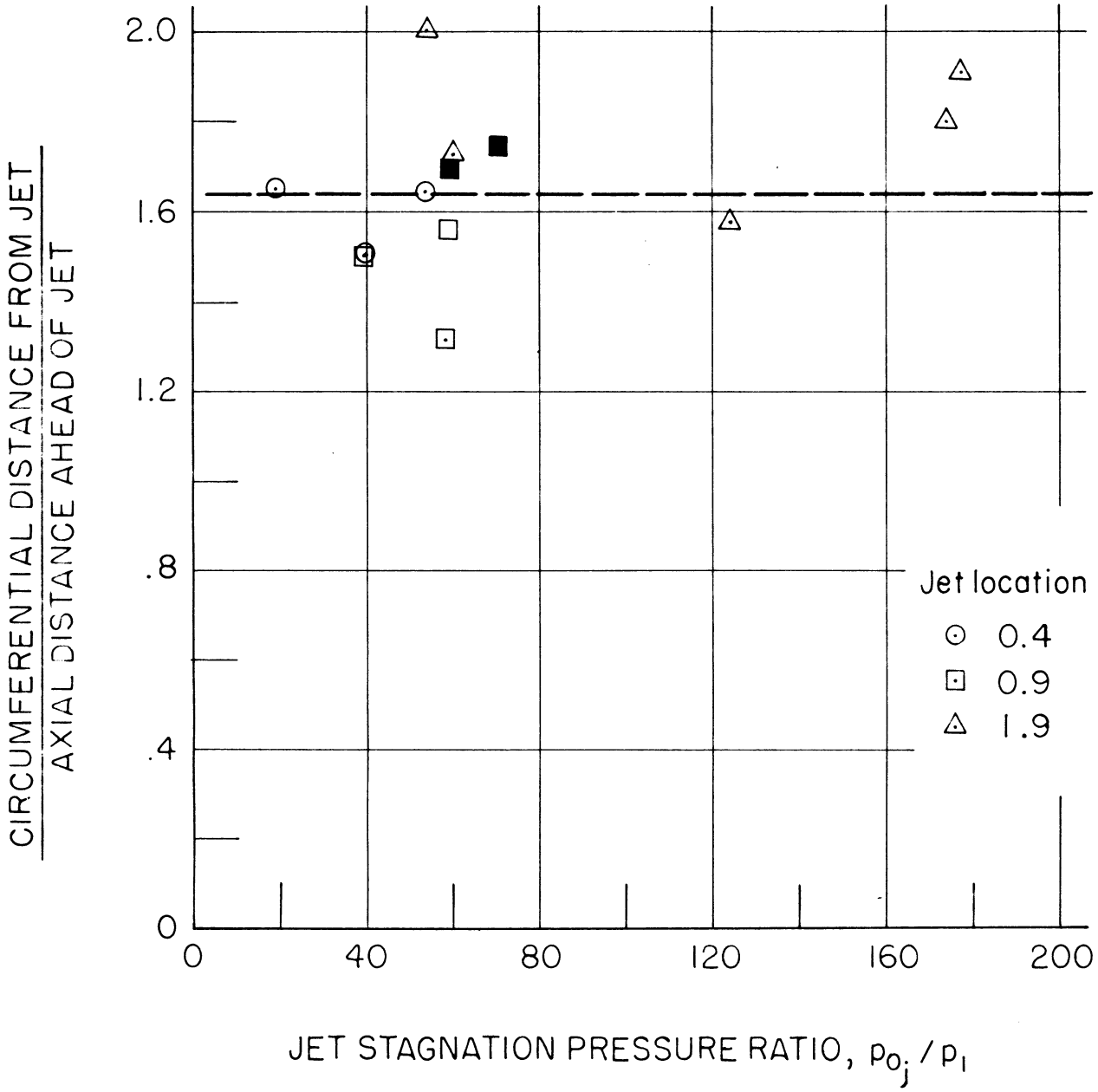

FIGURE 14. RATIO OF LATERAL TO LONGITUDINAL DISTANCES FROM JET LINE OF BOUNDARY - LAYER SEPARATION. SOLID SYMBOLS INDICATE TURBULENT BOUNDARY LAYER.
$M = 1.9$, $\alpha = 0$.

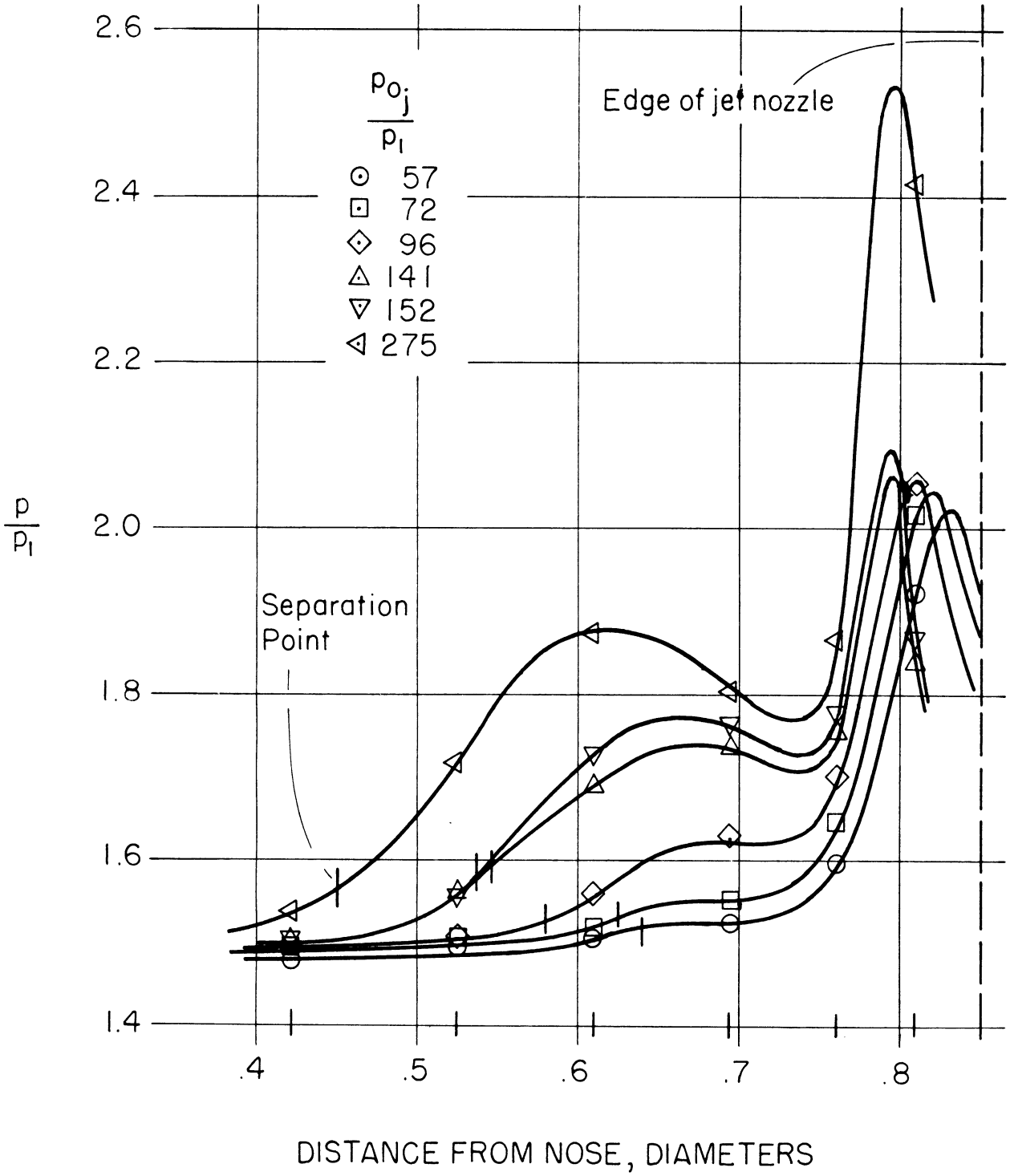

FIGURE 15. AXIAL PRESSURE DISTRIBUTION AHEAD OF JET.
$M = 1.9$, $\alpha = 0$.

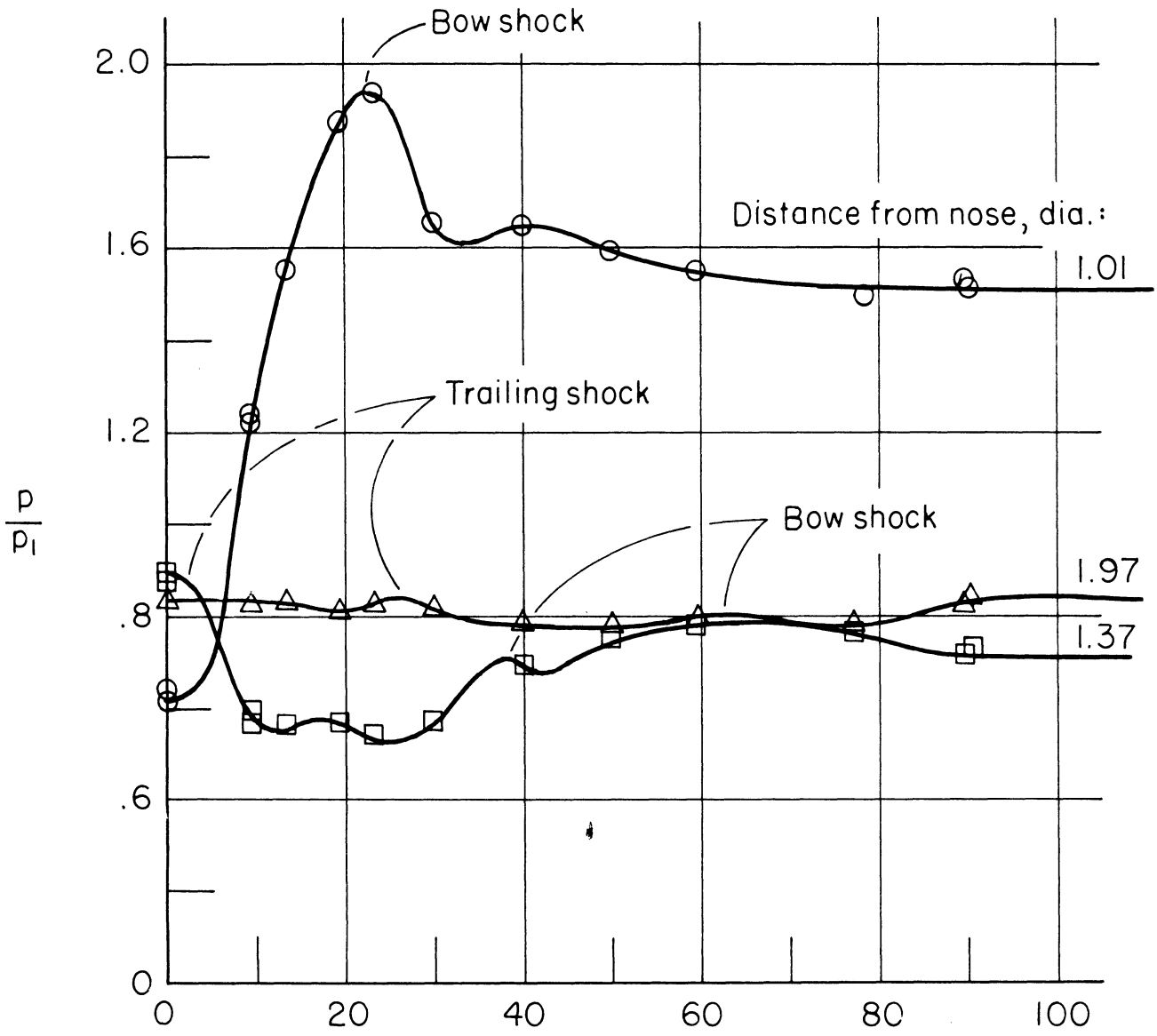

FIGURE 16. CIRCUMFERENTIAL PRESSURE DISTRIBUTION BEHIND JET. $M = 1.9$, $\alpha = 0$, $p_{0_j} / p_1 = 57$.

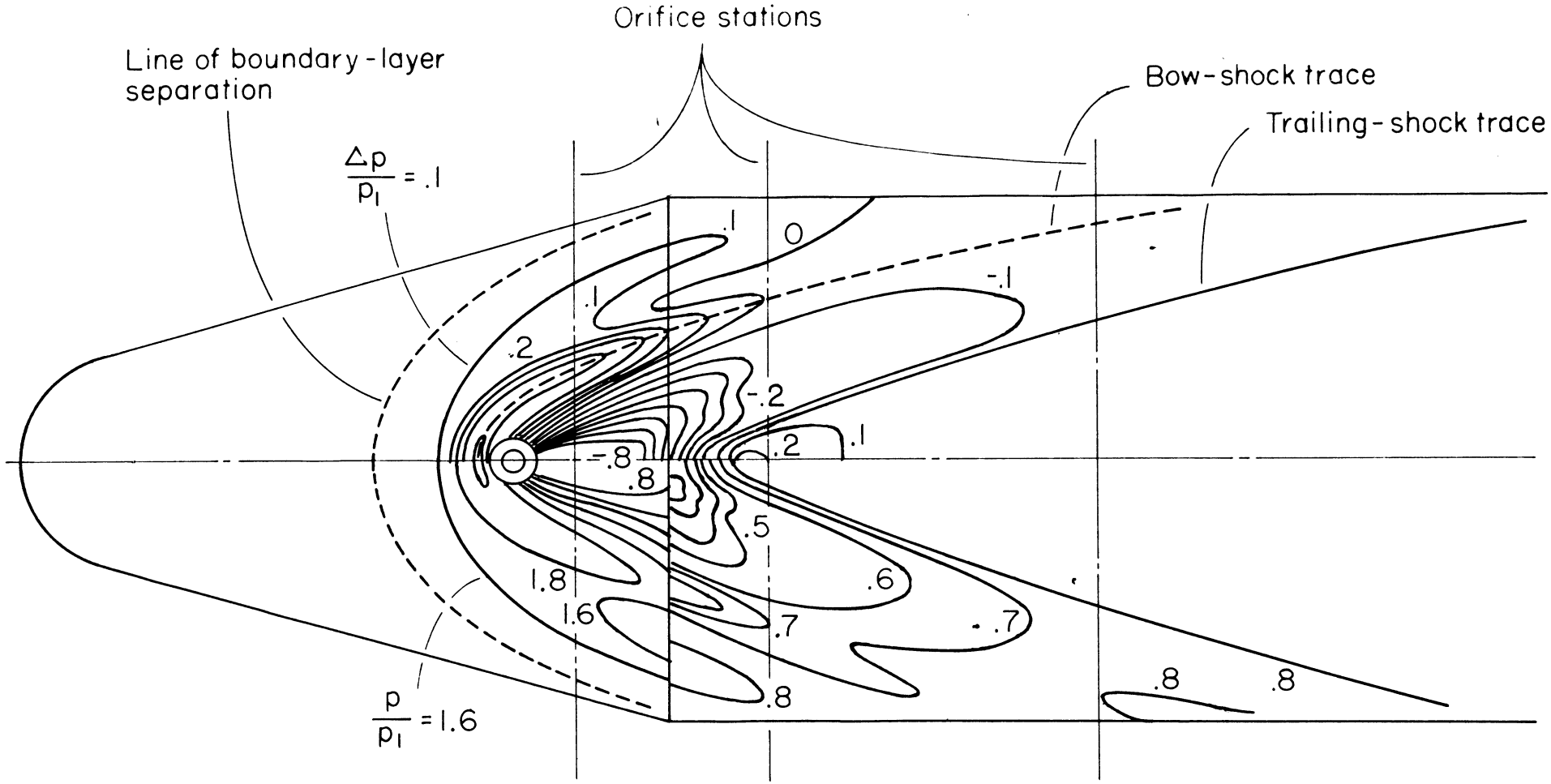

FIGURE 17. PRESSURE CONTOURS CONSTRUCTED FROM DATA OF FIGURE 15 AND 16. UPPER CONTOURS SHOW PRESSURE INCREMENTS DUE TO JET; LOWER CONTOURS SHOW PRESSURES. $M = 1.9$, $\alpha = 0$, $p_{0_j} / p_1 = 57$.

TABLE I.

Pressures Measured Ahead of Jet.
(Jet location = 0.9 diameters
from nose. M = 1.9. α = 0.)

Orifice		Values of p/p_1 at jet stagnation pressure of:					
Dist. From nose, diameters	Angle from jet, degrees	p_{o_j}/p_1 = 57	p_{o_j}/p_1 = 72	p_{o_j}/p_1 = 96	p_{o_j}/p_1 = 141	p_{o_j}/p_1 = 152	p_{o_j}/p_1 = 275
.422	0	1.476	1.487	1.496	1.500	1.502	1.537
.525	0	1.492	1.509	1.508	1.565	1.560	1.713
.610	0	1.503	1.515	1.559	1.688	1.728	1.877
.695	0	1.522	1.550	1.627	1.734	1.761	1.801
.761	0	1.595	1.642	1.699	1.753	1.773	1.864
.810	0	1.919	2.012	2.051	1.838	1.864	2.518
.453	60	1.487	1.496	1.504	1.500	1.508	1.499
.740	15	1.549	1.642	1.708	1.740	1.728	1.713

TABLE II.

Pressures Measured Behind Jet.
(Jet location = 0.9 diameters from nose. Jet stagnation pressure ratio p_{o_j}/p_1 = 57. M = 1.9. α = 0.)

Orifice angle from jet, degrees	Values of p/p_1 at orifice distance from nose of:		
	1.001 diameters	1.369 diameters	1.972 diameters
0	.606	.889	.832
0	.631	.878	.837
9.5	1.231	.568	.826
9.5	1.218	.590	.834
13.5	1.546	.558	.832
19.5	1.870	.563	.807
23.5	1.933	.536	.823
30	1.654	.568	.813
40	1.643	.687	.782
50	1.589	.749	.777
59.5	1.546	.779	.796
77	1.493	.764	.779
89.5	1.527	.706	.826
90	1.512	.718	.840
150	-----	.714	.824
180	1.541	.714	.824